CHAPTER
4 TWO AND THREE PHASE OPERATION OF BLDC MOTOR USING DIRECT TORQUE CONTROL

The budding demand for energy-efficient drives leads to the exploitation of permanent magnet motors as compared to the DC and AC motors. The finite inductance of the three-phase stator winding with only two-phase conducting does not allow the rise and fall rate of outgoing and incoming phase current to be equal resulting in the commutation torque ripple which deteriorates brushless DC motor performance. It is observed that the ripple in torque is large with 2-ΦO using conventional six-step BLDC motor control. The direct torque control (DTC) technique is considered to be an effectual method to reduce the commutation torque ripple and improve motor performance. This chapter provides a detailed analysis of conventional Six-Step DTC (SSDTC) techniques with 2-ΦO, Modified Six-Step DTC (MSSDTC) technique with 2-ΦO, conventional Twelve-Step DTC (TSDTC) technique with 2-3ΦO. Based on these three techniques, a Modified Twelve-Step DTC (MTSDTC) with PWMON and ONPWM control is proposed with 2-3ΦO to improve the BLDC motor performance with reduced torque ripple and switching losses as compared to the conventional DTC techniques.

4.1 Introduction

To improve the performance of motor two control methods (i) Field oriented control (FOC) (ii) Direct torque control(DTC) are widely used. DTC has found its impact in many industrial applications as well as in automotive industry due to its simple structure, no complex coordinate transformation requirement, less parameter dependency, no requirement of current regulator and fast torque response [14]. The idea of DTC was first developed by [62] and [63] in the mid 1980s for induction motor drives. It took around a decade for the analysis of this concept to be used for PMSM by [64]. A composite vector modulation DTC (CVM-DTC) technique is suggested by [65] for accurate torque and flux error compensation for PMSM during the steady state, dynamic state and transient state. The proposed method is compared with the conventional DTC and SVM-DTC. The results shows reduced torque ripples as compared to CDTC and improved dynamic response than the SVM-DTC. A hybrid control using the FOC and DTC technique for the sensorless operation of BLDC motor is suggested by[66] to acquaint the advantages of both the methods for improved motor performance. The DTC concept is incorporated for BLDC motor operated with only two phases conducting at a time by [67] by estimating electromagnetic motor torque in stationary reference frame using Clarke transformation for surface mounted permanent magnet machines. A direct torque control (DTC) technique with two phase conduction is suggested by [18] by designing a look up table for selection of voltage vectors operating the drive in constant torque region eliminating the flux control but no dead time compensation was incorporated.

A DTC technique with three phase conduction using pseudo-dq transformation is proposed by [68] for copper loss minimization. This is achieved by maximum torque per ampere (MTPA) control of BLDC motor to obtain high efficiency in electric vehicle. A comparison between a BLDC motor performance fed from conventional six switch inverter and a three switch inverter using FPGA is discussed by [69]. Better motor performance with reduced torque ripple is claimed with the new approach. An improved six step DTC technique with gating signals resembling unipolar PWM-ON technique with no requirement of dead time compensation over conventional six step DTC technique with reduced switching losses and improved motor performance is suggested by [70]. An enhanced control technique with PWM_ON_PWM mode by selection of non-zero and zero voltage vector is suggested by [71]. This mode of control provides reduced switching losses with 30^0 PWM before and after 60^0 conduction mode. A two-three phase operation with twelve voltage vectors DTC has been proposed by [72] to reduce the commutation torque ripple. The proposed technique is validated using the simulation results.

A combined two and three phase switching mode DTC technique is suggested by [73] for high speed operation to reduce the distortion of electromagnetic torque which produces torsion vibration to enhance the motor reliability. The three phase switching operation is suggested in the commutation region with positive torque error to equalize the rise rate and fall rate between the incoming and outgoing current. A two phase switching is incorporated with negative torque error in the commutation region apart from its operation in conduction region. To improve the reliability of the drive, the author [74] proposed a DTC technique using the null vectors for motor operation with the negative torque error for clockwise and anticlockwise motor operation in the conduction region and three phase switching mode with a three level torque controller for sector to sector transition for positive torque error.

This method provides an equalized switching frequencies between the upper and lower switches of the three phase inverter bridge and eliminate the common mode voltage (CMV). The overlap region angle in the commutation region is not mentioned by [70][73][74]. The twelve step DTC technique with 2-3ϕO is discussed by [75], which allows the conduction of the third switch in the overlap region based on the selection of overlap angle depending on the applied load and speed of the motor. The overlap angle was obtained using a trial and error method reducing the torque ripple, switching losses with improved drive efficiency. A parallel loop configuration for torque and velocity control using DTC (2+3P) operation for improved motor performance is suggested by[76] to reduces the steady state error of the speed. To validate the approach simulation results are provided.

A MTSDTC with ONPWM and PWMON control with a fixed overlap region of 15° and the zero switching concept with negative torque error unlike the conventional TSDTC technique with three-phase conduction in the commutation region or sector to sector transition is proposed for improved motor performance. The proposed approach is limited to torque control along with speed control with the motor operating in the constant torque zone below the base speed to reduce the commutation torque ripple for the smooth operation of the drive and counter clockwise rotation of the motor. The switching losses along with the elimination of dead band which needs much attention in conventional SSDTC and TSDTC techniques are reduced in the proposed techniques. The analysis and simulation for the proposed MTSDTC ONPWM and PWMON control with 2-3ΦO is analyzed and implemented using MATLAB®/SIMULINK environment. The steady-state and dynamic performance of the drive is tested on a prototype BLDC motor drive with HES and a shaft encoder to validate the simulation results.

4.2 **Principle of operation of DTC control**

Optimum torque control is achieved when the angle between stator flux linkage and rotor flux linkage be 90º in eq. (4.1).

$$\mathrm{T}_m = K_t \left|\psi_r\right|\left|\psi_s\right| Sin\delta \qquad 4.1$$

where,

K_t = torque constant,

ψ_r = rotor flux linkage,

Ψ_s = stator flux linkage,

δ = load angle or torque angle between the stator flux linkage and rotor flux linkage.

With the PM rotor, flux remain constant, the variation in torque is obtained by changing the stator voltage which incrementally changes the stator flux. The torque variation increases if the load angle δ increases. This necessitates faster rotation of the stator flux than the rotor flux. The rotor's speed determines how the flux produced by the rotor rotates. The stator flux should rotate at a slower pace than the rotor to minimise the load angle δ. Hence, for effective control of motor torque in eq. (4.1), the rotational speed of the stator flux vector needs to be controlled keeping its magnitude constant.

To accomplish the torque control using the above discussion, the three-phase stator windings are supplied with suitable voltage vectors. With the existing motor torque smaller than the reference value, voltage vectors that cause the stator flux vector to rotate in the same direction are chosen for anti-clockwise operation. The angle δ and real motor torque both rise as a result of this. When the actual motor torque exceeds the reference torque, the voltage vectors that cause the stator flux vector to rotate clockwise are selected. This can be done by choosing the active vectors. This leads to a decrease in the load angle δ which results in reduced motor torque. The torque and flux being the function of the applied stator voltage vector.

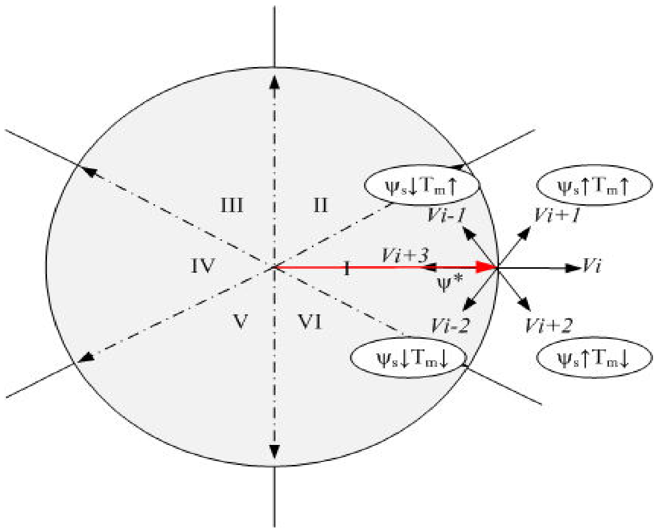

Fig. 4.1 Generalized theory of voltage vector selection

The voltage vector can be resolved into the direct component(flux) and indirect component (torque). Selecting the direct component of the stator flux vector changes the amplitude of the stator flux vector, while selecting the indirect component changes the rotating speed of the stator flux linkage. The closest voltage vector to the indirect component of the voltage vector is chosen to change the torque and for controlling the flux, the closest voltage vector near to the direct component is selected as discussed by [77].

From Fig.4.1, if the reference flux vector of the stator lies in the sector I, the positive direct components of the voltage vectors V_{i+1} and V_{i-1} enhance the amplitude of the stator flux, hence $\psi_s\uparrow$. V_{i+2} and V_{i-2} have a negative direct component which decreases the amplitude of the stator flux, hence $\psi_s\downarrow$. The voltage vectors V_{i+1} and V_{i+2} have a positive indirect component of the stator flux vector which increases the rotational speed of the stator flux vector and hence $T_m\uparrow$. Voltage vectors V_{i-1} and V_{i-2} have negative indirect components hence $T_m\downarrow$. The same theoretical concept for the voltage vector selection is used to develop the lookup tables prepared for 2-ΦO and 2-3ΦO of BLDC motor with DTC technique.

4.3 System description of DTC control of BLDC motor with 2-ΦO and 2-3ΦO

The basic block diagram of DTC of BLDC motor with twelve voltage vector selection within the six sector for 2-3ΦO is as shown in Fig.4.2. Controlling the amplitude and/or rotating speed of the stator flux vector can effectively control the electromagnetic torque. The three phase stator voltages and currents obtained in the abc phase variables needs to be transformed in to αβ coordinate system. Based on the obtained current and voltages the stator and rotor flux linkages are obtained which helps to decide the location of the stator voltage vector and electrical rotor position.

The BLDC motor with permanent magnet rotor requires an electronic commutator for supplying the three-phase stator winding. This is accomplished using a three-phase inverter bridge as shown in Fig.4.3. For BLDC motor operating with 120ºconduction mode of three-phase inverter bridge, at any time only two phases are conducting. It means only two switches one from the upper leg and one from the lower leg are turned on. No two switches from the same leg should be turned on as it will result in a short circuit of winding.

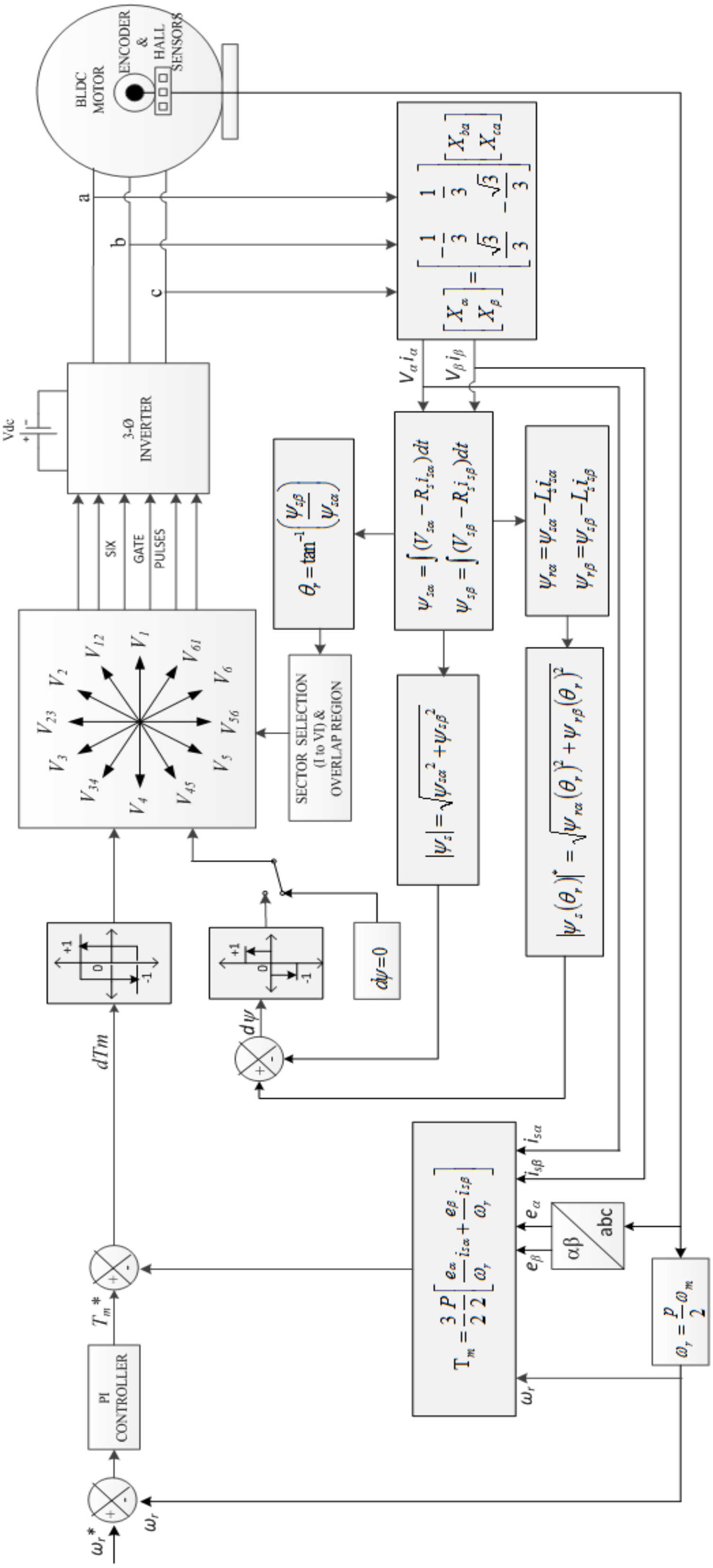

Fig. 4.2 Schematic diagram for the proposed MTSDTC technique

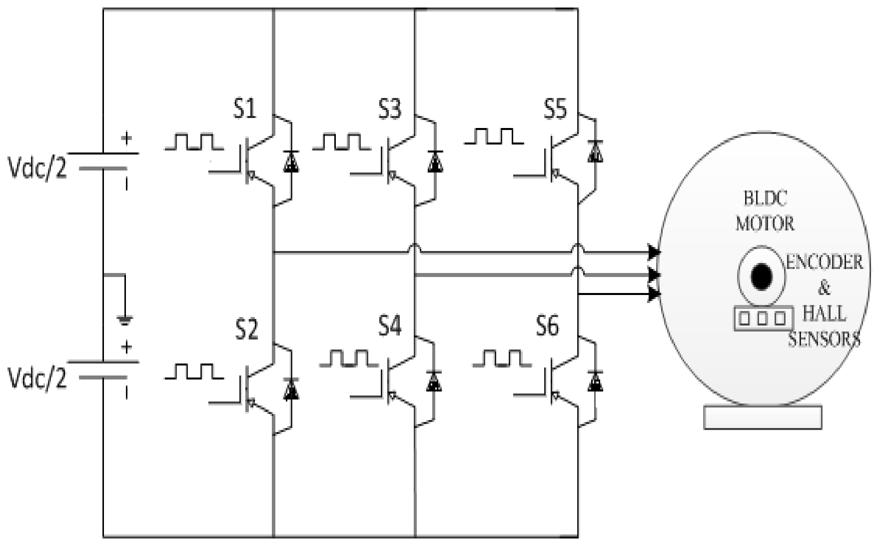

Fig. 4.3 Three-phase inverter circuit

The switching logic for the inverter switches is decided based on the torque error, flux linkage error, and electrical rotor position. For SSDTC(2-ΦO), six active voltage vectors, and for TSDTC and MTSDTC with 2-3ΦO, twelve voltage vectors are defined for BLDC motor. Various look up tables are provided for the commutation logic of the inverter circuit is discussed in detail in the mathematical modeling section. The electrical rotor position is obtained from the rotor flux linkages. The electromagnetic torque is derived based on the information of the back emf, stator currents and motor speed.

The DTC block diagram consists of a PI controller and two hysteresis controllers for closed-loop control. A two-level hysteresis controller is used for torque error correction and a three-level hysteresis controller for flux error correction. The flux and torque error are obtained by comparing the actual and reference quantities of flux and torque respectively. The rotation of the stator flux vector along with the reference vector is ensured by these hysteresis controllers. The actual motor speed can be obtained from the shaft encoder. This speed is compared with the reference speed. The error is processed by the PI controller. The PI controller is used to control the speed of the motor, the output of which gives the reference torque. For simplification, the flux error is considered to be zero making the drive operation in the constant torque region. For all DTC techniques, the only change that will occur in the block diagram is the lookup table developed for the selection of voltage vectors.

4.3.1 Mathematical modeling of direct torque controlled BLDC motor drive

The modelling of Direct torque-controlled BLDC motor drive is carried out in MATLAB®/ SIMULINK based on the

- Torque estimation
- Stator flux estimation
- Sector selection
- Switching logic table for voltage vector selection
- Transformation of voltage, current, and back emf in the stationary reference frame (Clarke transformation)

The three-phase stator winding is supplied through a three-phase inverter bridge which acts as an electronic commutator for the BLDC motor. The switching logic for the 3-Φ inverter bridge is based on the value of torque error, flux linkage error, and the sector in which the stator flux vector lies. Each phase conducts for 120 electrical degrees. For DTC, the abc phase variables of the BLDC motor are transformed into αβ coordinates using Clark's Transformation as explained below in the stationary reference frame. Electromagnetic torque calculation in the stationary reference frame is given by

$$T_m = \frac{3}{2}\frac{p}{2}\left[\frac{e_\alpha}{\omega_r} i_{s\alpha} + \frac{e_\beta}{\omega_r} i_{s\beta}\right] \qquad 4.2$$

Where,

ω_r=electrical rotor speed

$e_\alpha, e_\beta, i_{s\alpha}, i_{s\beta}$ = $\alpha\beta$ axes back emf and stator currents

To obtain the $\alpha\beta$ component of current, voltage, and back emf, Clarke transformation has to be used The generalized form is

$$\begin{bmatrix} X_\alpha \\ X_\beta \end{bmatrix} = \frac{2}{3}\begin{bmatrix} 1 & -1/2 & -1/2 \\ 0 & \sqrt{3}/2 & -\sqrt{3}/2 \end{bmatrix}\begin{bmatrix} X_a \\ X_b \\ X_c \end{bmatrix} \qquad 4.3$$

With star-connected stator winding with floating neutral, at any instant, only two phases are conducting. By neglecting the zero sequence components in a balanced three-phase system, a more simplified 2*2 Clarke transformation[18] is further used.

$$\begin{bmatrix} X_\alpha \\ X_\beta \end{bmatrix} = \begin{bmatrix} -\frac{1}{3} & \frac{1}{3} \\ \frac{\sqrt{3}}{3} & -\frac{\sqrt{3}}{3} \end{bmatrix} \begin{bmatrix} X_{ba} \\ X_{ca} \end{bmatrix} \tag{4.4}$$

Where, X represents back emf, current, and voltage. In the stationary reference frame, the stator voltage equation is as follows

$$\begin{aligned} V_{s\alpha} &= R_s i_{s\alpha} + L_s \frac{di_{s\alpha}}{dt} + \frac{d\psi_{r\alpha}}{dt} \\ V_{s\beta} &= R_s i_{s\beta} + L_s \frac{di_{s\beta}}{dt} + \frac{d\psi_{r\beta}}{dt} \end{aligned} \tag{4.5}$$

$$\begin{aligned} \psi_{r\alpha} &= \psi_{s\alpha} - L_s i_{s\alpha} \\ \psi_{r\beta} &= \psi_{s\beta} - L_s i_{s\beta} \end{aligned} \tag{4.6}$$

Where,

$V_{s\alpha}$, $V_{s\beta}$ = $\alpha\beta$ axis stator phase voltages

R_s , L_s = $\alpha\beta$ axis stator resistance and inductance

$\psi_{s\alpha}$, $\psi_{s\beta}$ = $\alpha\beta$ axes stator flux linkage

$\psi_{r\alpha}$, $\psi_{r\beta}$ = $\alpha\beta$ axes rotor flux linkage

$\psi_{s\alpha}$, $\psi_{s\beta}$ are obtained by integrating eq. (4.5) on both the sides.

$$\begin{aligned} \psi_{s\alpha} &= \int (V_{s\alpha} - R_s i_{s\alpha}) dt \\ \psi_{s\beta} &= \int (V_{s\beta} - R_s i_{s\beta}) dt \end{aligned} \tag{4.7}$$

The magnitude of the stator flux vector is obtained as

$$|\psi_s| = \sqrt{\psi_{s\alpha}^2 + \psi_{s\beta}^2} \quad 4.8$$

The reference stator flux linkage command is obtained using the rotor flux linkages as given below

$$|\psi_s(\theta_r)|^* = \sqrt{\psi_{r\alpha}(\theta_r)^2 + \psi_{r\beta}(\theta_r)^2} \quad 4.9$$

$|\psi_s(\theta_r)|^*$ = reference stator flux linkage command. It varies with the electrical rotor position θ_r. The angular rotor position is obtained from

$$\theta_r = \tan^{-1}\left(\frac{\psi_{s\beta}}{\psi_{s\alpha}}\right) \quad 4.10$$

4.3.2 Analysis of conventional DTC technique with 2-ΦO

A change in torque can be achieved for DTC control of the BLDC motor in two-phase conduction by keeping the amplitude of the stator flux linkage constant and raising the rotational speed of the stator flux linkage as quickly as possible. This helps to reduce the complexity of the drive. The conventional six-step DTC technique consists of six non-zero and two zero space vectors. For proper commutation of three-phase stator windings, six non-zero voltage vectors are defined. The stator phase voltages Van, Vbn, and Vcn are decided by the status of the six switches, S1, S2, S3, S4, S5, and S6. For this six non-zero voltage space vectors are defined for the BLDC motor. These voltage vectors are 60º apart. They are V1(100001) which represents, S1 and S6 are ON; V2(001001) i.e S3 and S6 are ON; V3(011000) i.e S2 and S3 are ON; V4(010010) i.e S2 and S5 are ON; V5(000110) i.e S4 and S5 are ON and V6(100100) i.e S1 and S4 are ON in the conduction region as shown in Fig. 4.4.

The selection of the voltage vector depends on the output signals obtained from flux and torque hysteresis controllers as well as the sector in which the voltage vector lies. Here the magnitude of the stator flux vector is kept constant. When there is a negative torque error and the actual torque exceeds the reference, a voltage vector is determined that keeps the stator flux vector heading in the opposite direction. The computational logic table for the conventional SSDTC technique is as shown in Table 4.1 and for the MSSDTC technique is given in Table 4.3. The six voltage vectors and the commutation logic for inverter switching for the SSDTC is given in Table 4.2. If the reference flux vector lies in sector 1, from the theory discussed in section 4.2, voltage vector V2 is selected to increase the torque response by increasing the rotational speed of the voltage vector and V5 is selected to decrease the rotational speed to decrease the torque response. In MSSDTC, the concept of zero switching is introduced by selecting voltage vector V2'. This technique helps to improve the drive performance by reducing the torque ripple and increasing efficiency by reduced switching losses.

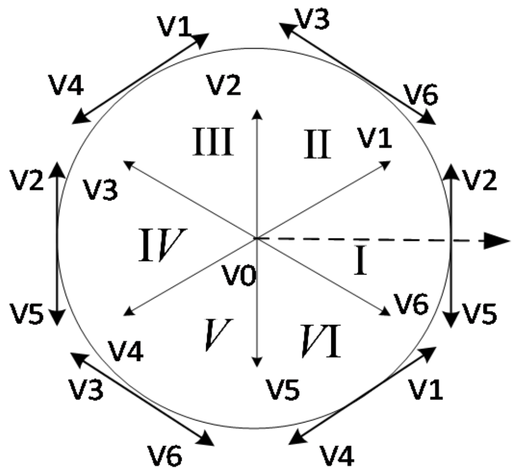

Fig. 4.4 SSDTC stator flux linkage space vector representation

Table 4.1 Computational logic table for conventional SSDTC

Steps		1	2	3	4	5	6
		Sector	Sector	Sector	Sector	Sector	Sector
ψ	T_m	I	II	III	IV	V	VI
0	1	V2	V3	V4	V5	V6	V1
0	-1	V5	V6	V1	V2	V3	V4

Table 4.2 Voltage vectors and inverter switching for SSDTC

Voltage Vector		Inverter Switches						3-Phases		
		S1	S2	S3	S4	S5	S6	A	B	C
V1	100001	1	0	0	0	0	1	+		-
V2	001001	0	0	1	0	0	1		+	-
V3	011000	0	1	1	0	0	0	-	+	
V4	010010	0	1	0	0	1	0	-		+
V5	000110	0	0	0	1	1	0		-	+
V6	100100	1	0	0	1	0	0	+	-	

Table 4.3 Computational logic table for MSSDTC

Steps		1 Sector	2 Sector	3 Sector	4 Sector	5 Sector	6 Sector
ψ	T_m	I	II	III	IV	V	VI
0	1	V2	V3	V4	V5	V6	V1
0	-1	V2' (001000)	V3' (010000)	V4' (000010)	V5' (000100)	V6' (100000)	V1' (000001)

4.3.3 Analysis of twelve-step DTC technique

To reduce torque ripple produced in the commutation region due to the mismatch in the slope of a outgoing current and incoming current, a third switch is made ON in the overlap region. The voltage vector selection for the 2-3ΦO with TSDTC technique based on the location of the reference flux vector is as shown in Fig. 4.5. The twelve switching states for the 2-3ΦO of BLDC motor are as shown in Fig. 4.6.

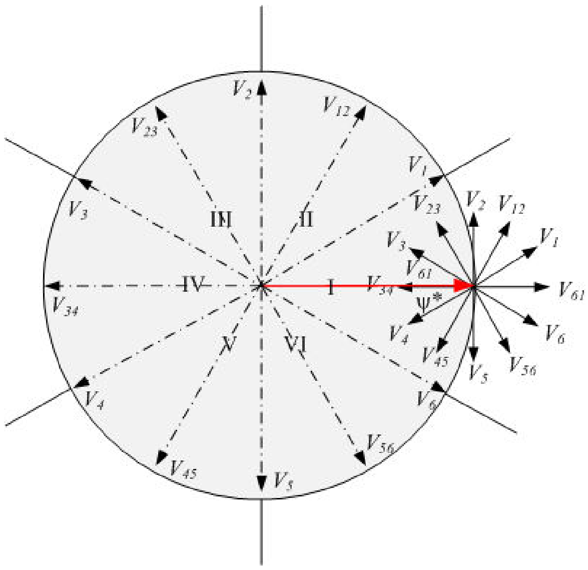

Fig. 4.5 For the TSDTC approach, voltage vector selection with the stator reference flux vector in sector I

In TSDTC, apart from the conventional SSDTC control, six more voltage vectors are defined for the overlap regions as V12(101001), V23(011001), V34(011010), V45(010110), V56(100110), V61(100101). With the twelve-step DTC, three switches are turned ON in the overlap region. The commutation region for 2-ΦO is 60° with a conduction region of 120°. Here an optimum overlap region of 15° is considered. In this overlap region switching ON the third switch, makes the inactive phase active to reduce the torque ripple.

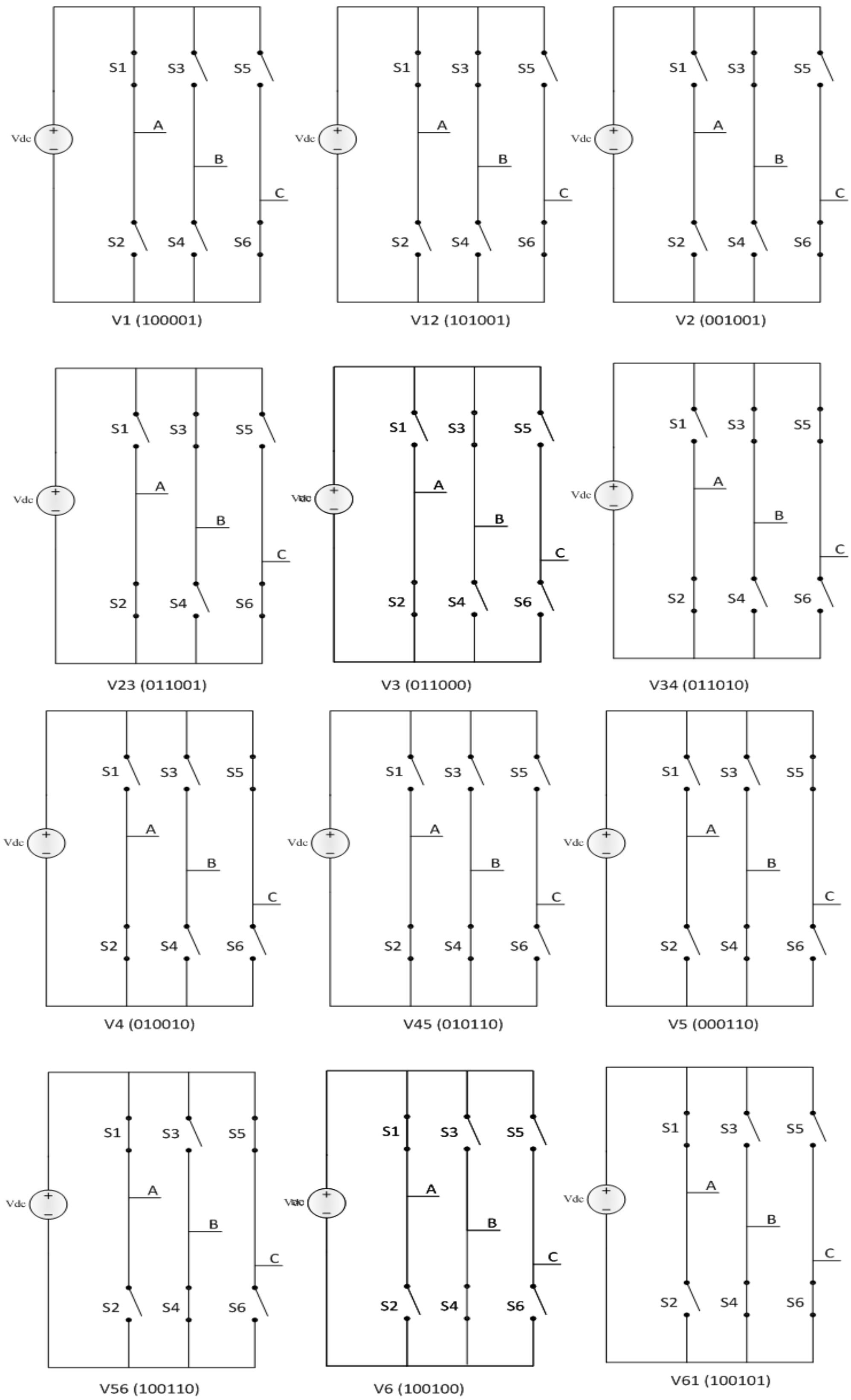

Fig. 4.6 Three-phase inverter circuit operation with twelve-step DTC technique

This reduces the equivalent winding inductance which results in reduced current ripple and hence torque ripple. These voltage space vectors for the TSDTC technique are represented as shown in Fig.4.7. The same logic that is used in SSDTC for voltage vector selection is used in TSDTC for selecting the voltage vectors. If torque error is positive means actual torque is less than the reference torque within the predefined hysteresis band, a voltage vector that increases the speed of the stator flux linkage in a counter-clockwise direction must be selected. For negative torque error, a voltage vector that reduces the speed of stator flux linkage is selected.

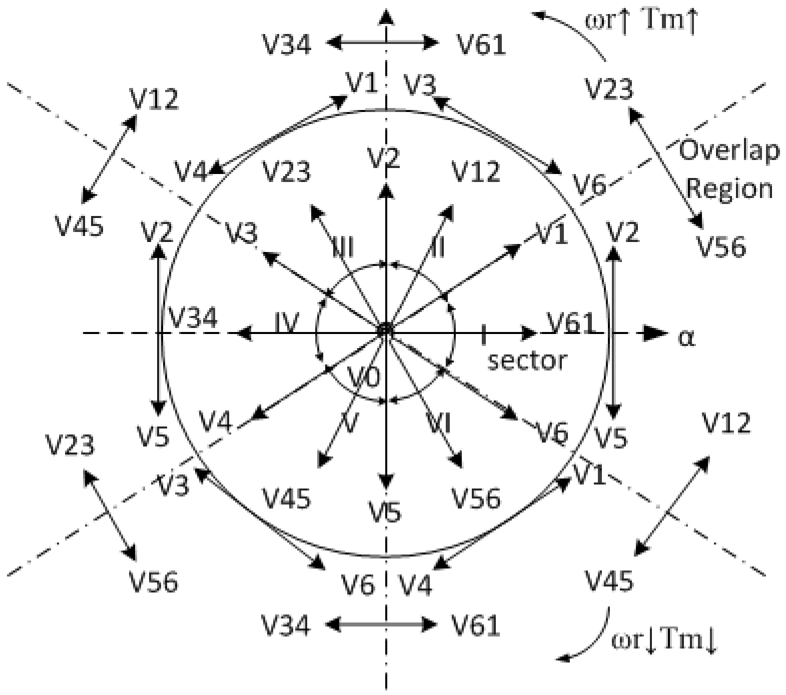

Fig. 4.7 Phasor representation of the twelve voltage vectors defined for six sectors and the overlap region

The computational logic table based on Fig. 4.7 is created in Table 4.4 based on which the commutation logic for selection of inverter switching operation is as shown in Table 4.5. In TSDTC, with positive torque error in the sector I, voltage vector V2(001001) is selected in the conduction region making two inverter switches S3 and S6 ON. With negative torque error voltage vector V5(000110) is selected making Switch S4 and S5 conduct. In the overlap region voltage vector V23(011001) is selected for positive torque error making the three switches S2, S3, and S6 ON to increase the speed of the reference vector in the anti-clockwise direction. With negative torque error in the overlap region voltage vector V56(100110) is selected reducing the speed of the reference vector in the clockwise direction. This technique helps to reduce the commutation torque ripple as compared to the conventional SSDTC technique.

Table 4.4 Computational logic table for conventional TSDTC

Steps		1	2	3	4	5	6	7	8	9	10	11	12
		sector	Overlap region	sector	Overlap region	sector	Overlap region	sector	Overlap region	sector	Overlap region	sector	Overlap region
ψ	T_m	I	I-II	II	II-III	III	III-IV	IV	IV-V	V	V-VI	VI	VI-I
0	1	V2	V23	V3	V34	V4	V45	V5	V56	V6	V61	V1	V12
0	-1	V5	V56	V6	V61	V1	V12	V2	V23	V3	V34	V4	V45

Table 4.5 Voltage vectors and inverter switching for conventional TSDTC

Voltage Vector		Inverter Switches						3-Phases			Overlap Region Voltage Vector		Inverter Switches						3-Phases		
		S1	S2	S3	S4	S5	S6	A	B	C			S1	S2	S3	S4	S5	S6	A	B	C
V1	100001	1	0	0	0	0	1	+		-	V12	101001	1	0	1	0	0	1	+	+	-
V2	001001	0	0	1	0	0	1		+	-	V23	011001	0	1	1	0	0	1	-	+	-
V3	011000	0	1	1	0	0	0	-	+		V34	011010	0	1	1	0	1	0	-	+	+
V4	010010	0	1	0	0	1	0	-		+	V45	010110	0	1	0	1	1	0	-	-	+
V5	000110	0	0	0	1	1	0		-	+	V56	100110	1	0	0	1	1	0	+	-	+
V6	100100	1	0	0	1	0	0	+	-		V61	100101	1	0	0	1	0	1	+	-	-

4.3.4 Analysis of MTSDTC with ONPWM and PWMON

In the conventional six-step DTC technique, during high-speed operation, the outgoing current decays at a faster rate than the incoming current producing a dip in the non-commutating phase current resulting in to ripple in motor torque. By implementing the tho phase conduction mode in the commutation region with a positive torque error, the current is allowed to flow through a controllable switch whose duty can be adjusted to reduce torque ripple. For a low-speed operation, the outgoing current takes more time to decay than the incoming current, again resulting in the dip in non- commutating current resulting in the dip in current ripple and hence torque ripple. [66] had discussed four types of unipolar PWM techniques for a three-phase inverter bridge.

By using the unipolar PWM technique, only one switch is supplied by a PWM signal and the other switch of the same phase leg is OFF. This nullifies the chance of a short circuit of one phase leg and no dead time compensation is required between the two switches of the same phase leg which is a must in the bipolar PWM technique. This technique helps to reduce the torque ripple and improves drive operation.

In the MTSDTC PWMON technique for positive torque error the voltage vector for inverter switching remains the same but for negative torque error the inverter switching changes in both conduction and commutation region with only one switch conducting considering an optimum 15° overlap region. The phasor representation of voltage vector selection for the MTSDTC ONPWM and PWMON technique is as shown in Fig.4.8.

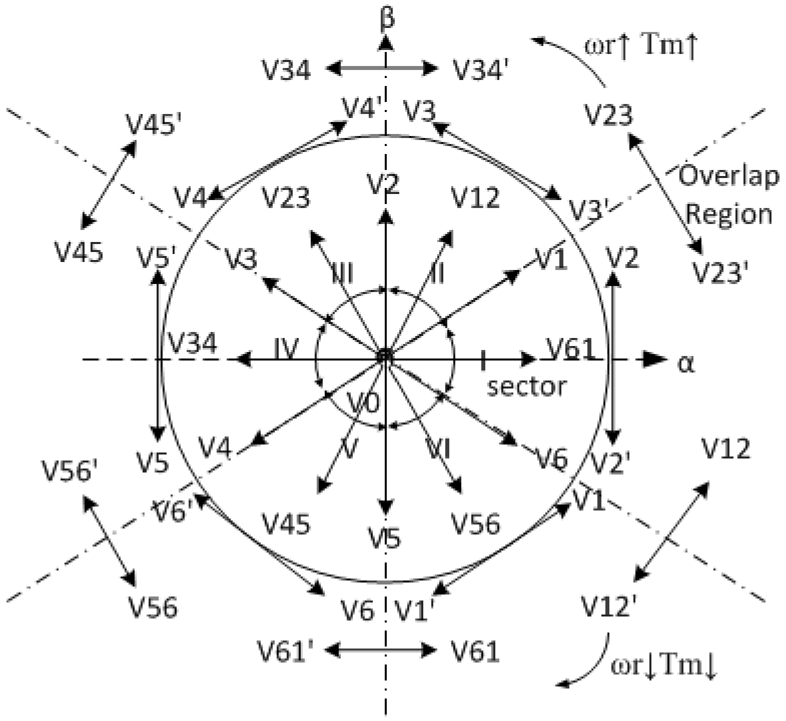

Fig. 4.8 Phasor representation of voltage vector selection for the MTSDTC ONPWM and PWMON technique

In the MTSDTC ONPWM technique, when the actual torque is less than the reference torque which means positive torque error, voltage vector V2(001001) is selected for the three-phase inverter bridge with switch S3 and S6 ON to increase the speed of the stator voltage vector in sector I and voltage vector V23(011001) with three switch conducting in the overlap region is same as TSDTC. But when actual torque is greater than the reference torque which means torque error is negative, voltage vector V2'(001000) in the sector I and voltage vector V23' (010000) in the overlap region is selected making only one switch to operate. The computational logic table for modified TSDTC with ONPWM and PWMON technique for anti-clockwise rotation of the BLDC motor is as given in Table 4.6. Though the computational table looks to be the same for both the approach but the voltage vectors defined for negative torque error are different as mentioned in Table 4.7. and Table 4.8. respectively for ONPWM and PWMON techniques. At all times when torque error is negative only one switch is conducting with current commutation being done using one switch and two diodes. This method reduces the switching losses in the conduction as well as commutation region as well as the torque ripple in the commutation region due to decreased winding inductance.

To get an insight on how the current commutation takes place and how the transition of current takes place, the switching of inverter circuit with 2-ΦO in the conduction region and then 3-ΦO in the commutation region as well the switching of inverter switches in the conduction region with positive and -ve torque error is shown in Fig 4.9. The inverter switching states in from transition of the reference vector from sector V to sector VI and in the overlap region between sector V and VI is as shown in Fig.4.9. During the ON state in sector V with positive torque error the motor operates with 2-ΦO with switch S1 and S4 ON. With negative torque error, the OFF state is accomplished by switch S1 and a diode. In the overlap region between sectors V and VI, with positive torque error, the third switch S6 along with S1 and S4 is turned ON. This makes the current flow in all the three stator winding during the ON state. Again with negative torque error, only one switch S6 is turned ON with two diodes in OFF condition. The whole commutation process is completed by the transfer of current from switch S4 to S6 in the conduction region. By using this switching logic, the uni-polar PWM pulses with ONPWM are generated which reduces the switching losses.

In the TSDTC PWMON technique, when the actual torque is less than the reference torque which means positive torque error, voltage vector V2(001001) is selected to increase the speed of the stator voltage vector in sector I and voltage vector V23(011001) with three switches conducting in overlap region same as that with ONPWM. But when actual torque is greater than the reference torque which means torque error is negative, voltage vector V2'(000001) in sector I and voltage vector V23' (000001) in the overlap region is selected as shown in Table 4.8.

Table 4.6 Computational logic table for MTSDTC ONPWM and MTSDTC PWMON

Steps		1	2	3	4	5	6	7	8	9	10	11	12
		sector	Overlap region	sector	Overlap region	sector	Overlap region	sector	Overlap region	sector	Overlap region	sector	Overlap region
ψ	T_m	I	I-II	II	II-III	III	III-IV	IV	IV-V	V	V-VI	VI	VI-I
0	1	V2	V23	V3	V34	V4	V45	V5	V56	V6	V61	V1	V12
0	-1	V2'	V23'	V3'	V34'	V4'	V45'	V5'	V56'	V6'	V61'	V1'	V12'

Table 4.7 Voltage vectors and inverter switching for MTSDTC ONPWM

Voltage Vector		Inverter Switches						3-Phases			Voltage Vector		Inverter Switches						3-Phases		
		S1	S2	S3	S4	S5	S6	A	B	C			S1	S2	S3	S4	S5	S6	A	B	C
V1	100001	1	0	0	0	0	1	+		-	V1'	000001	0	0	0	0	0	1			-
V2	001001	0	0	1	0	0	1		+	-	V2'	001000	0	0	1	0	0	0		+	
V3	011000	0	1	1	0	0	0	-	+		V3'	010000	0	1	0	0	0	0	-		
V4	010010	0	1	0	0	1	0	-		+	V4'	000010	0	0	0	0	1	0			+
V5	000110	0	0	0	1	1	0		-	+	V5'	000100	0	0	0	1	0	0		-	
V6	100100	1	0	0	1	0	0	+	-		V6'	100000	1	0	0	0	0	0	+		
V12	101001	1	0	1	0	0	1	+	+	-	V12'	001000	0	0	1	0	0	0		+	
V23	011001	0	1	1	0	0	1	-	+	-	V23'	010000	0	1	0	0	0	0	-		
V34	011010	0	1	1	0	1	0	-	+	+	V34'	000010	0	0	0	0	1	0			+
V45	010110	0	1	0	1	1	0	-	-	+	V45'	000100	0	0	0	1	0	0		-	
V56	100110	1	0	0	1	1	0	+	-	+	V56'	100000	1	0	0	0	0	0	+		
V61	100101	1	0	0	1	0	1	+	-	-	V61'	000001	0	0	0	0	0	1			-

A similar selection of the voltage vectors is done in the conduction and overlap region. The computational logic table for the inverter switching state operation according to the voltage vectors is the same as given in Table 4.6 for the conduction and the overlap region for the 12 step operation. The voltage vectors and inverter switching for MTSDTC PWMON are as given in Table 4.8. To get an insight on how the current commutation takes place and how the transition of current takes place with the MTSDTC PWMON technique, the switching of inverter circuit with 2-ΦO in the conduction region and then 3-ΦO in the commutation region as well the switching of inverter switches in the conduction region with positive and -ve torque error is shown in Fig 4.9.

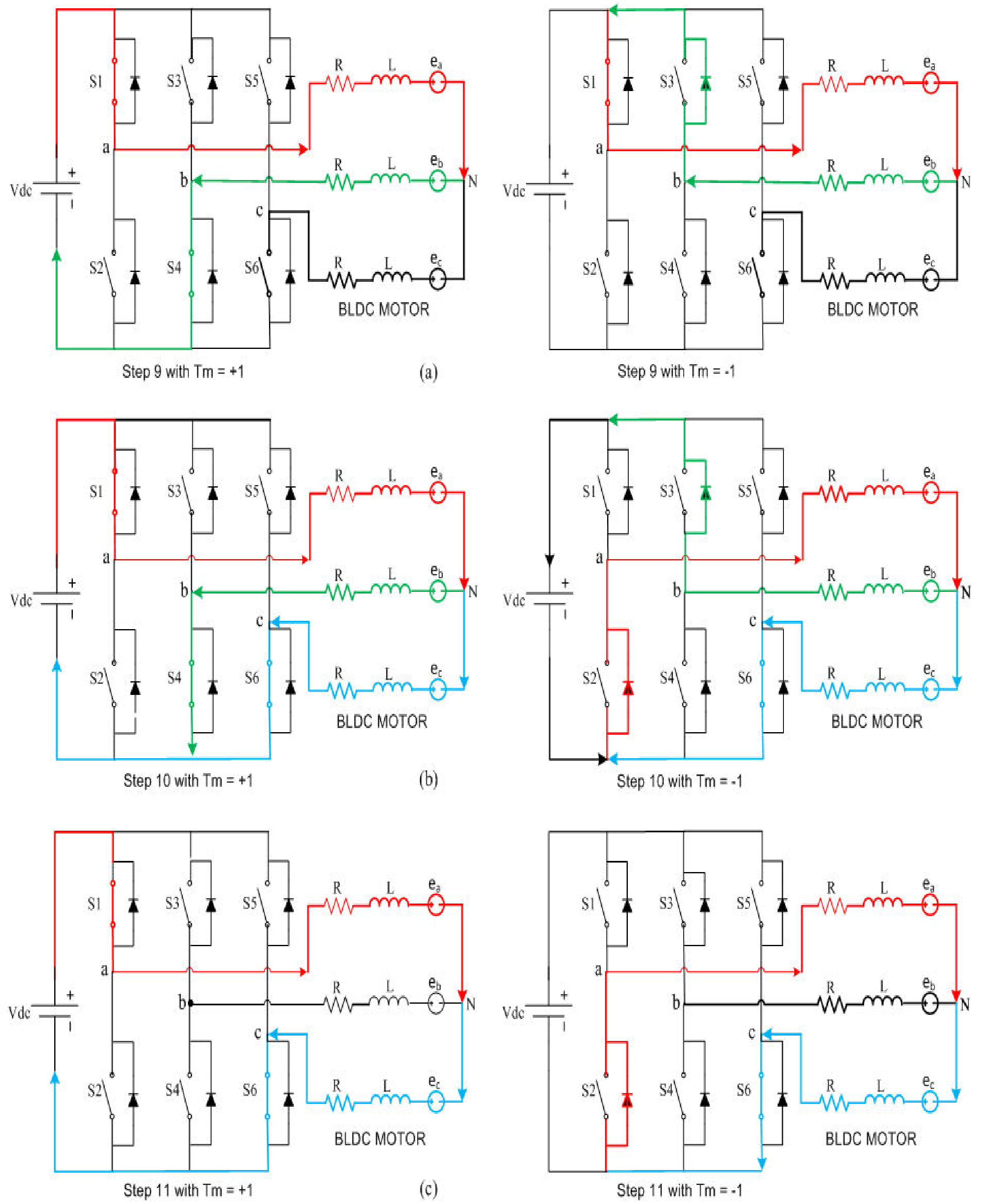

Fig. 4.9 BLDC motor inverter switching states with the MTSDTC ONPWM control in the (a)conduction region (b)commutation region and (c) conduction region with +ve and -ve with torque error

The inverter switching states from transition of the reference vector from sector V to sector VI and in the overlap region between sector V and VI is as shown in Fig.4.10. Three steps 9,10 and 11 are considered from Table 4.8. During the ON state in sector V with positive torque error the motor operates with 2-ΦO with switch S1 and S4 ON. With negative torque error, the OFF is accomplished by switch S1 and a diode. In the overlap region between sectors V and VI, with positive torque error, the third switch S6 along with S1 and S4 is turned ON. This makes the current flow in all the three stator winding during the ON state. Again with negative torque error, only one switch S4 is turned ON with two diodes during the OFF condition. The whole commutation process is completed by the transfer of current from switch S4 to S6 in the conduction region.

Unlike the TSDTC technique in which three inverter switches are turned ON in the commutation region with positive and negative torque error, using the proposed switching logic, the uni polar PWM pulses with PWMON and ONPWM techniques are generated which reduces the switching losses. In the MTSDTC PWMON technique for positive torque error the voltage vector for inverter switching remains the same but for negative torque error the inverter switching changes in both conduction and commutation region with only one switch conducting considering an 15° overlap region. The MTSDTC ONPWM switching logic helps to reduce the commutation torque ripple which improves motor performance.

Table 4.8 Voltage vectors and inverter switching for MTSDTC PWMON

Voltage Vector		Inverter Switches						3-Phases			Voltage Vector		Inverter Switches						3-Phases		
		S1	S2	S3	S4	S5	S6	A	B	C			S1	S2	S3	S4	S5	S6	A	B	C
V1	100001	1	0	0	0	0	1	+		-	V1'	100000	1	0	0	0	0	0	+		
V2	001001	0	0	1	0	0	1		+	-	V2'	000001	0	0	0	0	0	1			-
V3	011000	0	1	1	0	0	0	-	+		V3'	001000	0	0	1	0	0	0		+	
V4	010010	0	1	0	0	1	0	-		+	V4'	010000	0	1	0	0	0	0	-		
V5	000110	0	0	0	1	1	0		-	+	V5'	000010	0	0	0	0	1	0			+
V6	100100	1	0	0	1	0	0	+	-		V6'	000100	0	0	0	1	0	0		-	
V12	101001	1	0	1	0	0	1	+	+	-	V12'	100000	1	0	0	0	0	0	+		
V23	011001	0	1	1	0	0	1	-	+	-	V23'	000001	0	0	0	0	0	1			-
V34	011010	0	1	1	0	1	0	-	+	+	V34'	001000	0	0	1	0	0	0		+	
V45	010110	0	1	0	1	1	0	-	-	+	V45'	010000	0	1	0	0	0	0	-		
V56	100110	1	0	0	1	1	0	+	-	+	V56'	000010	0	0	0	0	1	0			+
V61	100101	1	0	0	1	0	1	+	-	-	V61'	000100	0	0	0	1	0	0		-	

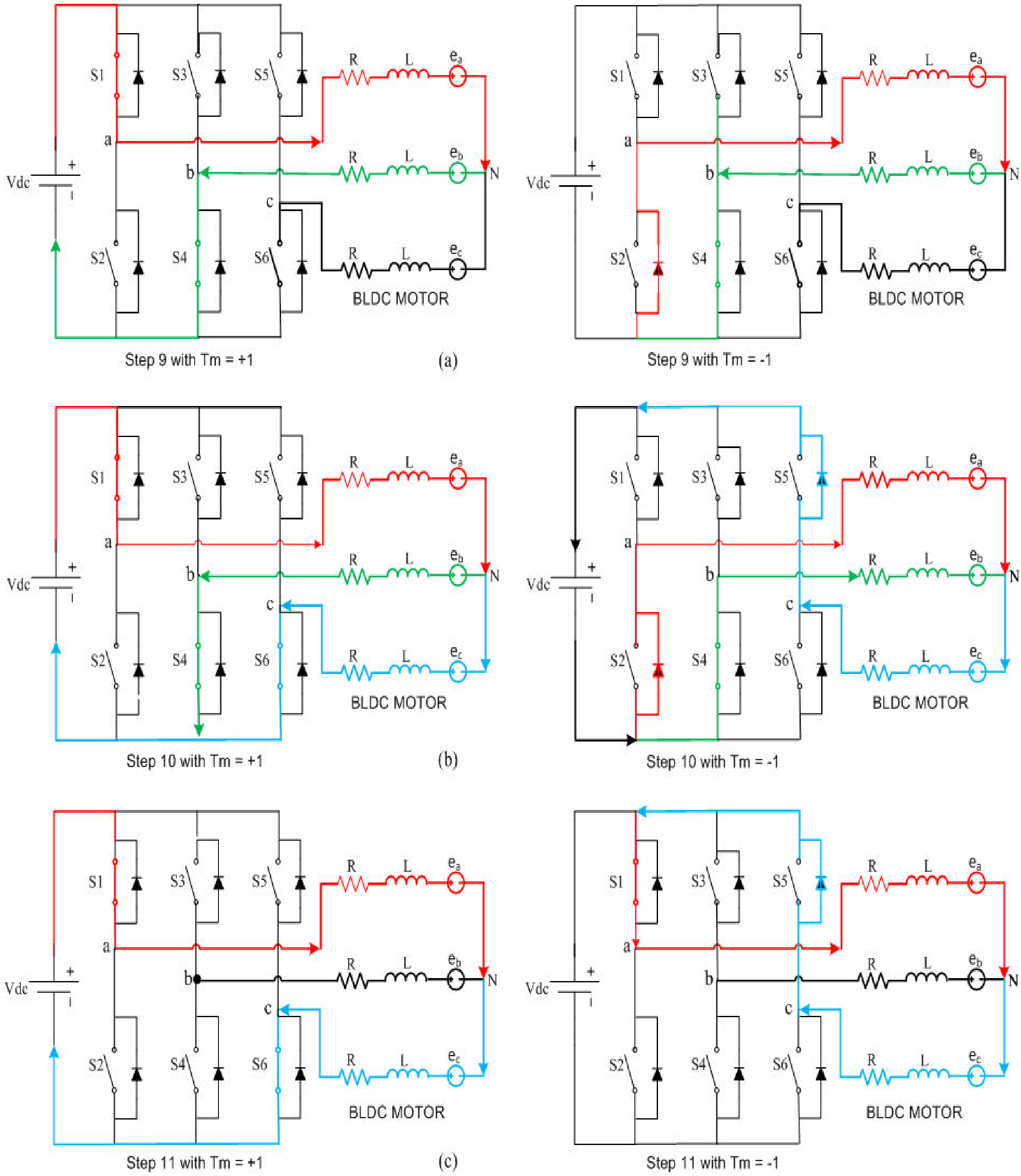

Fig.4.10 Inverter switching states of BLDC motor for the MTSDTC PWMON control with the transition of the voltage vector from sector V to sector VI.

4.4 Simulation result and discussion of all DTC techniques

The simulation is performed for six type of DTC control technique listed as (a) SSDTC (b)MSSDTC (c)TSDTC (d)MTSDTC ONPWM (e)MTSDTC ONPWM using MATLAB®/SIMULINK to compare the performance of the BLDC motor drive under different speed and load conditions. The commutation logic tables provided in the previous sections are used to produce the six gate pulses for the three-phase inverter bridge for all the techniques as shown in Fig. 4.11. The proposed switching logic for MTSDTC with 2-3ΦO produces the same switching pulses with the MSSDTC with 2-ΦO. It can be observed that the switching losses are reduced with the MSSDTC, MTSDTC ONPWM, and MTSDTC ONPWM. The motor speed set at 500rpm. At time t=0.2 sec the set speed is changed to 1000rpm. Again at time t= 0.4 sec, the motor speed is increased to 2000rpm as shown Fig. 4.12. It is observed that the time taken by the controller to reach the set speed is very less. From Fig 4.13 and Fig. 4.14 it can be depicted that the motor oscillates more to settle at the set speed with TSDTC and SSDTC method. The settling time is more with the MTSDTC ONPWM and PWMON The settling time is less with the MSSDTC, MTSDTC with ONPWM and PWMON method with the speed change from 500 rpm to 1000 rpm. With applied speed change from 1000 rpm to 2000 rpm the settling time with the MSSDTC, MTSDTC with ONPWM and PWMON method is reduced. The drive oscillates whenever a change in speed occurs with the TSDTC and SSDTC techniques.

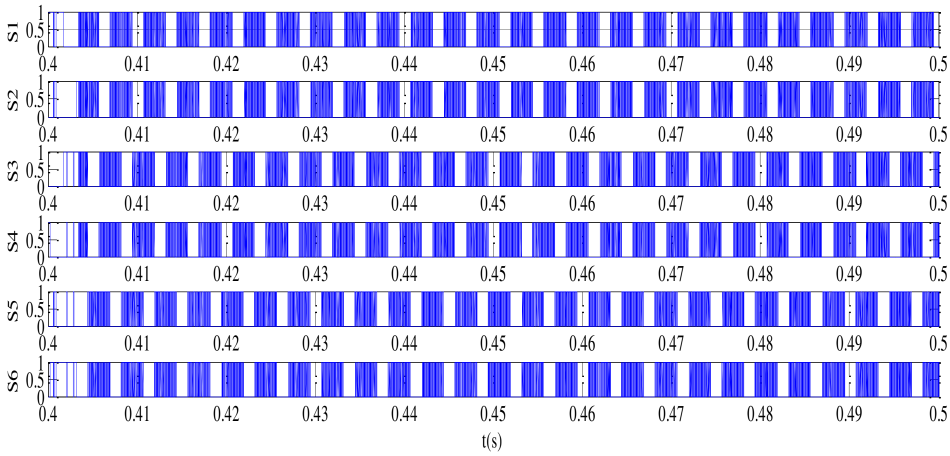

(a)

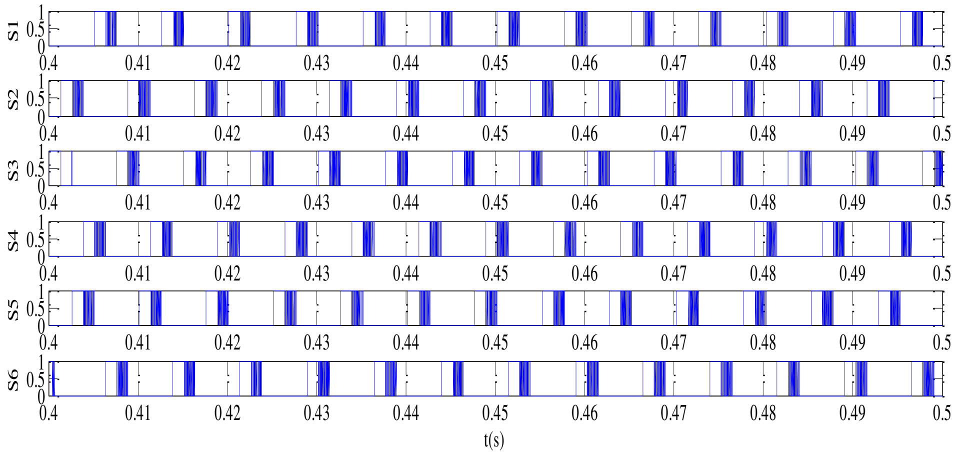
S1
S2
S3
S4
S5
S6
0
0.5
1
0.4
0.41
0.42
0.43
0.44
0.45
0.46
0.47
0.48
0.49
0.5
t(s)

(b)

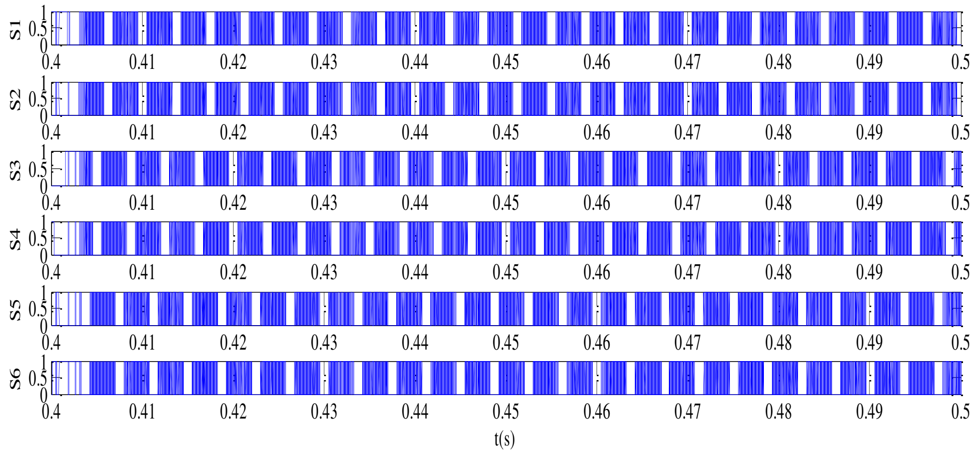
S1
S2
S3
S4
S5
S6
0
0.5
1
0.4
0.41
0.42
0.43
0.44
0.45
0.46
0.47
0.48
0.49
0.5
t(s)

(c)

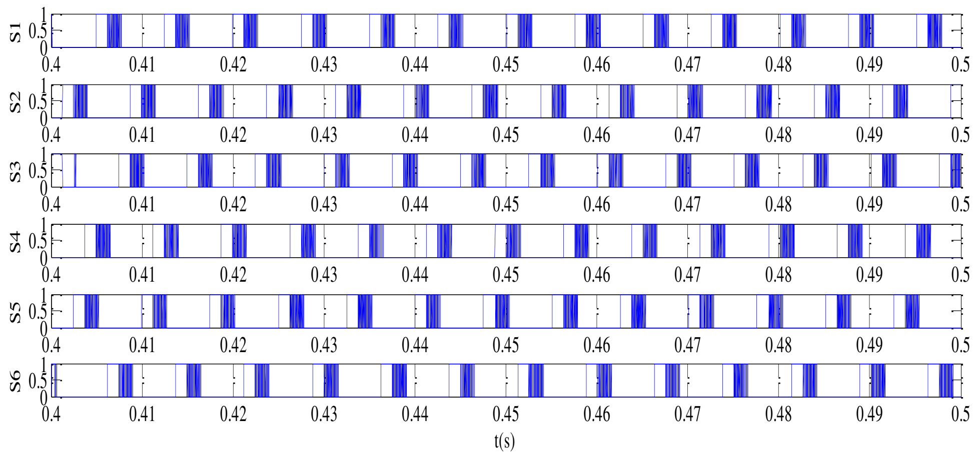
S1
S2
S3
S4
S5
S6
0
0.5
1
0.4
0.41
0.42
0.43
0.44
0.45
0.46
0.47
0.48
0.49
0.5
t(s)

(d)

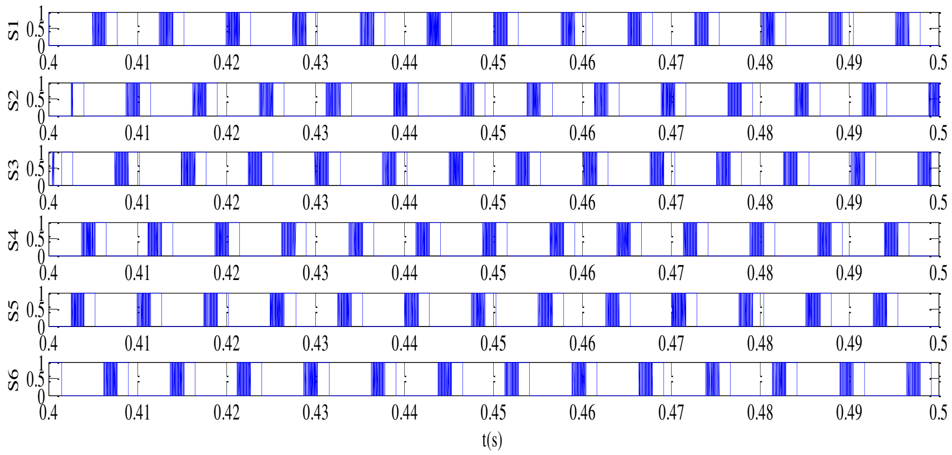

(e)

Fig. 4.11 Gate pulses for inverter switches with (a)SSDTC (b)MTSDTC (c)TSDTC (d)MTSDTC ONPWM (e)MTSDTC PWMON

The variation in motor electromagnetic torque and stator current with a change in load torque is as shown in Fig. 4.15 and Fig. 4.16 respectively. An initial load of 0.6 Nm is applied and with an increase in load at 0.25 sec to 1.2 Nm. The effect of this change in load can be observed on the current with all the techniques at a is shown in Fig. 4.16. The motor speed is changed from 1000rpm to 2000rpm. The magnitude of the stator current changes with the change in load.

To analyze the effect of the conducting phase current on the non-conducting phase current, the zoomed results are projected. A Zoomed view of phase current at a speed of 1000rpm and 2000rpm for (a) MTSDTC PWMON (b)MTSDTC ONPWM (c) TSDTC is shown in Fig. 4.17 and 4.18 respectively. As discussed in chapter 2, it can be observed that a ripple in current is produced in the non-commutating phase current with the mismatch in the rate of incoming and outgoing currents. This ripple in non-commutating current is reflected as commutation torque ripple in the motor torque. At higher speed, the current ripple is distinctive with MTSDTC PWMON and TSDTC as compared to the MTSDTC ONPWM control as shown in Fig.4.18. This current ripple is responsible to produce the commutation torque ripple.

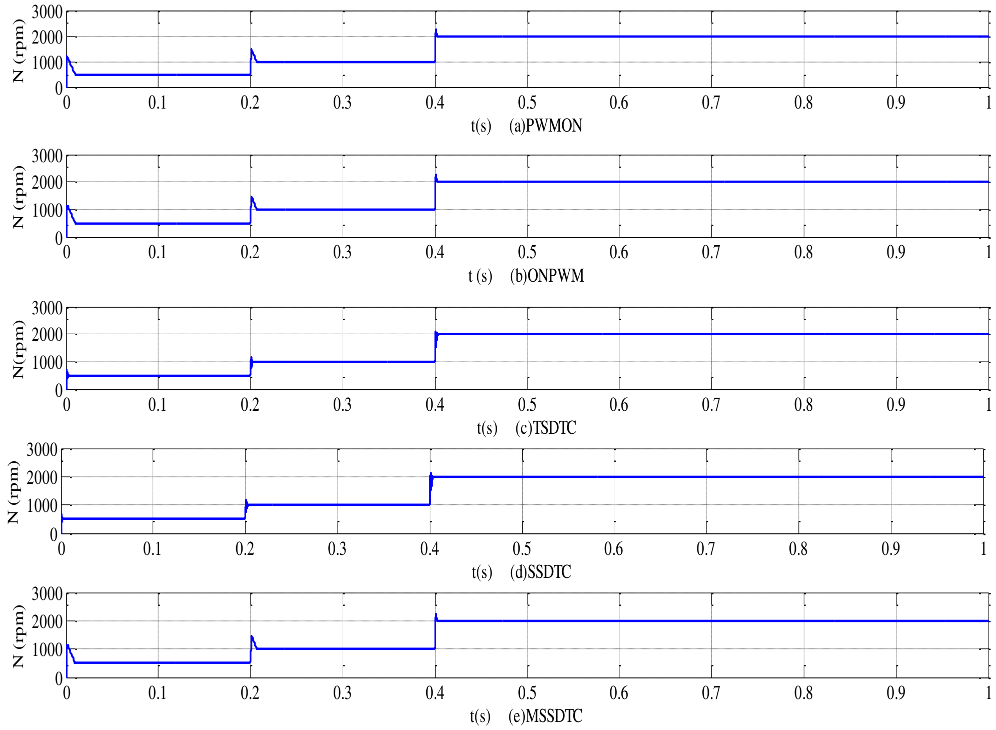

Fig. 4.12 Variable speed operation of bldc drive with a set speed of 500 rpm , 1000 rpm and 2000 rpm with a load of 1.2 Nm

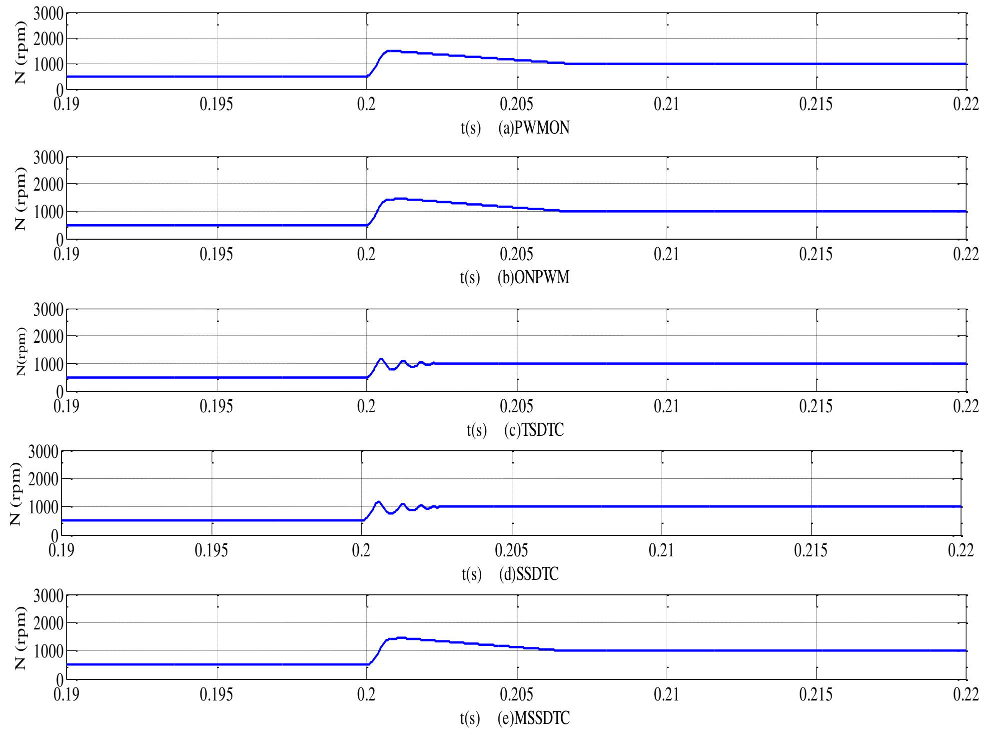

Fig. 4.13 Zoomed view of speed change from 500rpm to 1000rpm

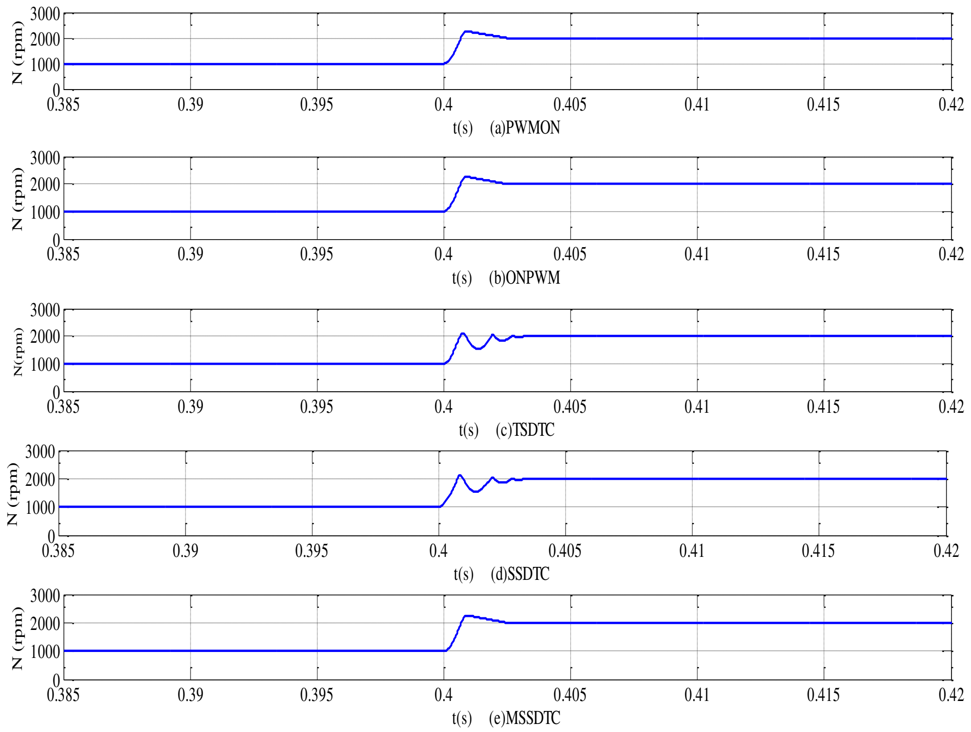

Fig. 4.14 Zoomed view of speed change from 1000rpm to 2000 rpm

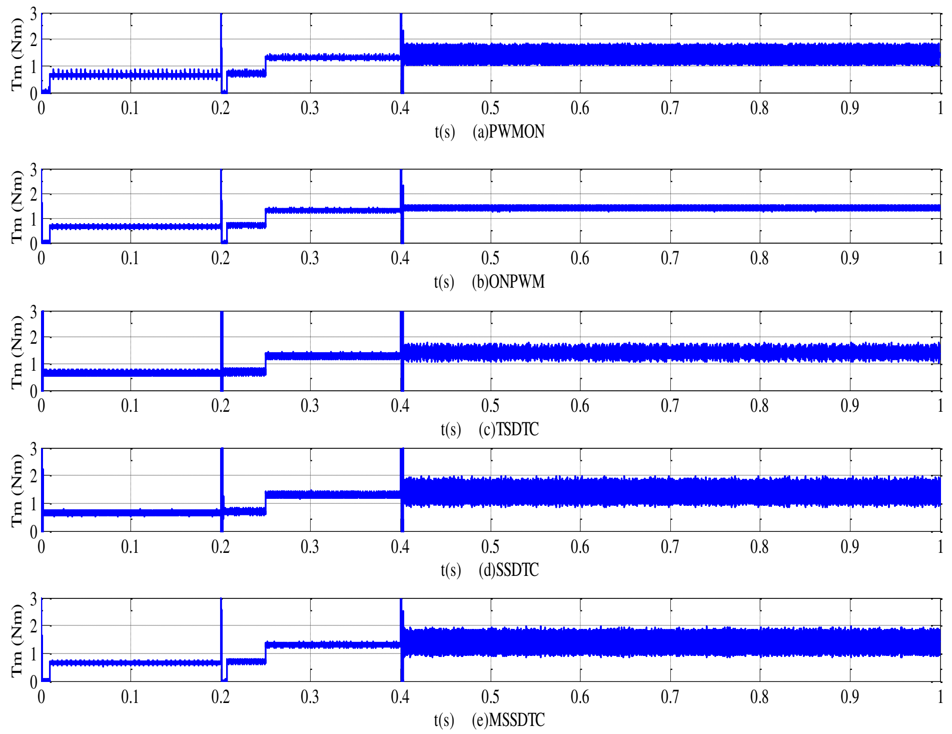

Fig. 4.15 Variation in the electromagnetic torque with an initial load of 0.6 Nm and with an increase in load at 0.25 sec to 1.2 Nm

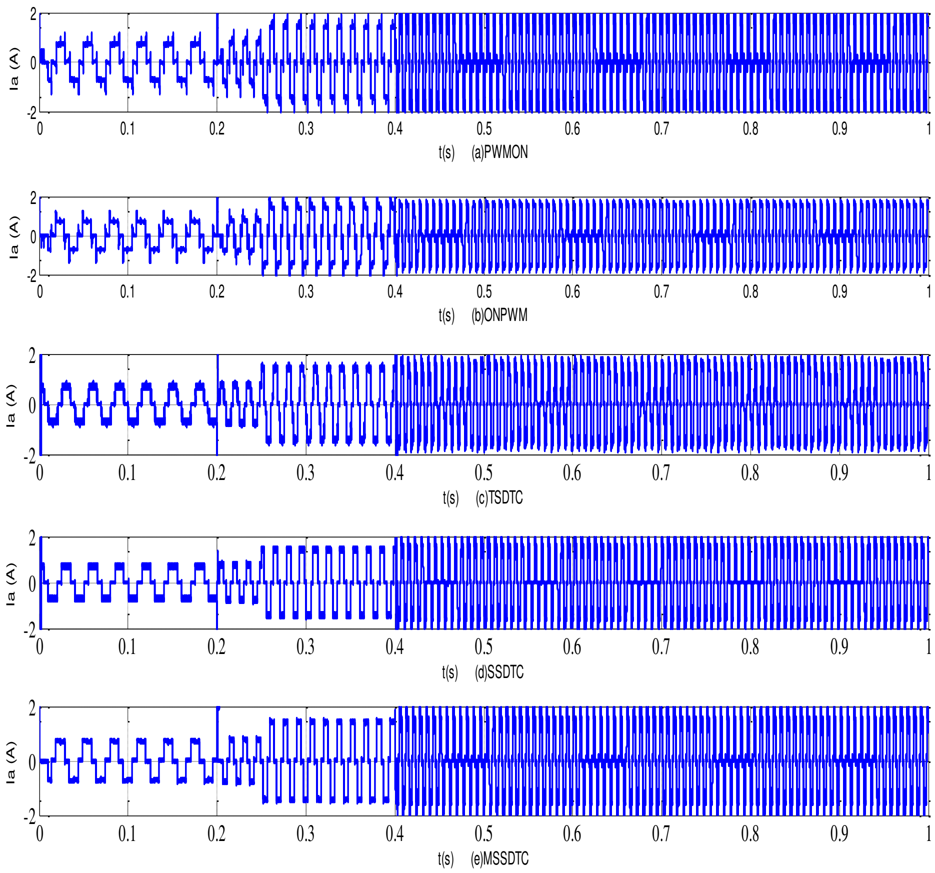

Fig. 4.16 Variation in motor phase current with applied speed change and load

Similarly, with a lower speed of 500 rpm and 1000 rpm, the commutation torque is almost the same as conduction torque as shown in Fig.4.19 and Fig.4.20. At a speed of 2000 rpm, the torque ripple is high for all the other methods other than ONPWM control as shown in Fig.4.21. The slope of incoming and outgoing current is same resulting in no dip in the non conducting current. The conduction as well as the commutation torque is reduced with the ONPWM technique. The torque ripple effects the motor performance to a great extent in applications which requires the smooth drive operation. Stator flux linkage plots for all the DTC techniques are as shown in Fig. 4.22. The trajectory of the flux linkage is found to be more smooth with the modified MTSDTC ONPWM and MSSDTC techniques among all the curves to provide improved motor performance with smooth operation. A comparative analysis is prepared from the simulation results to analyze all the DTC techniques is tabulated in Table 4.9.

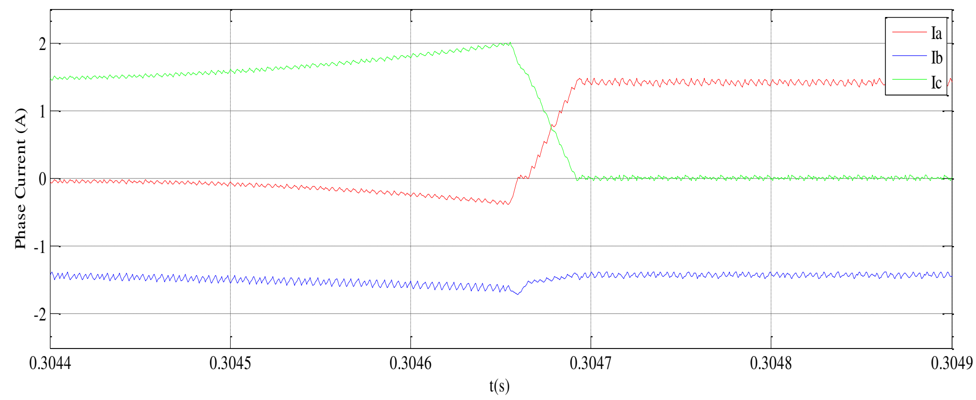

(a)

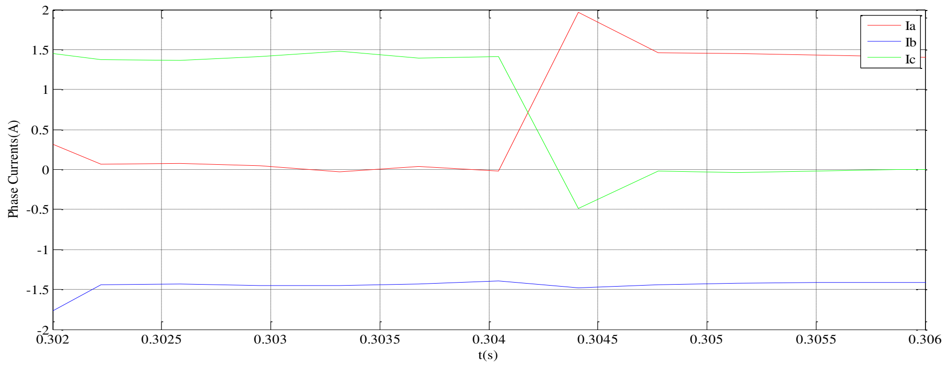

(b)

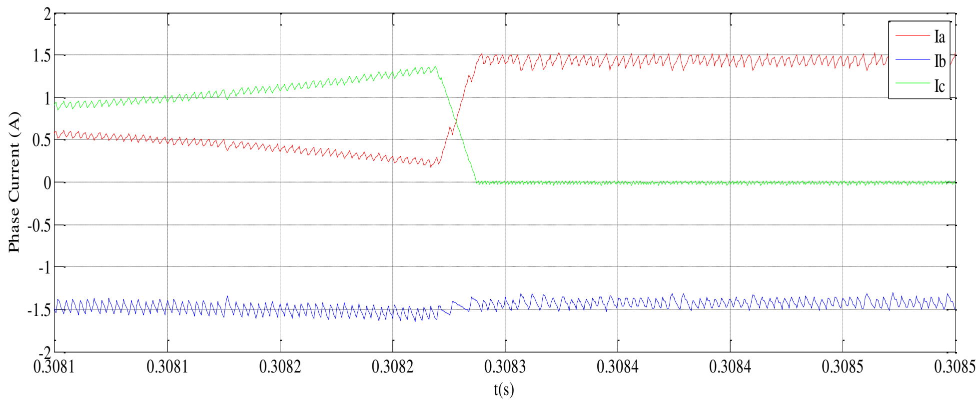

(c)

Fig. 4.17 Zoomed view of phase current at a speed of 1000 rpm (a) MTSDTC PWMON (b)MTSDTC ONPWM (c) TSDTC

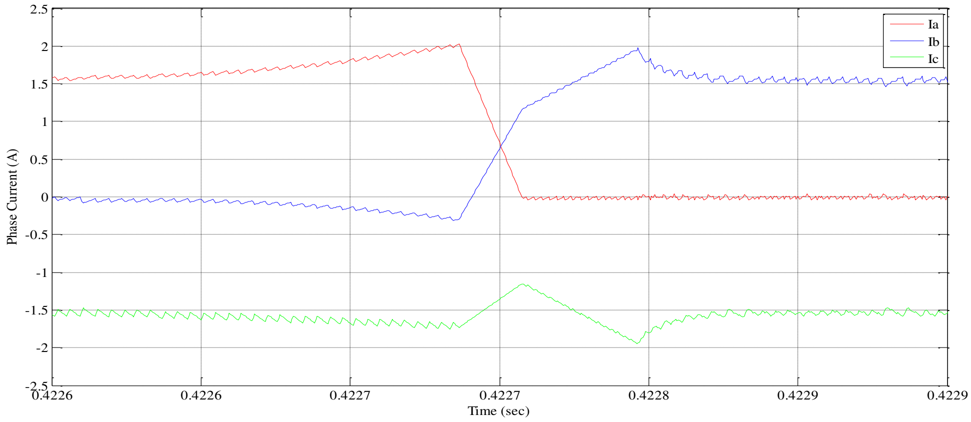

(a)

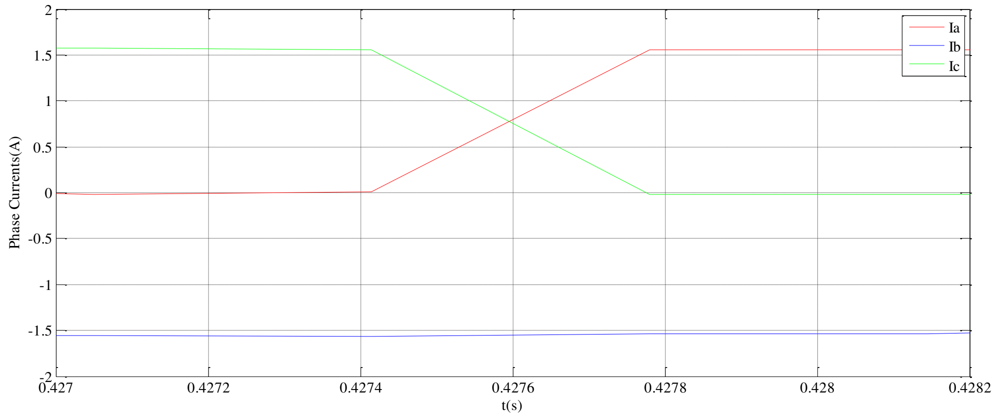

(b)

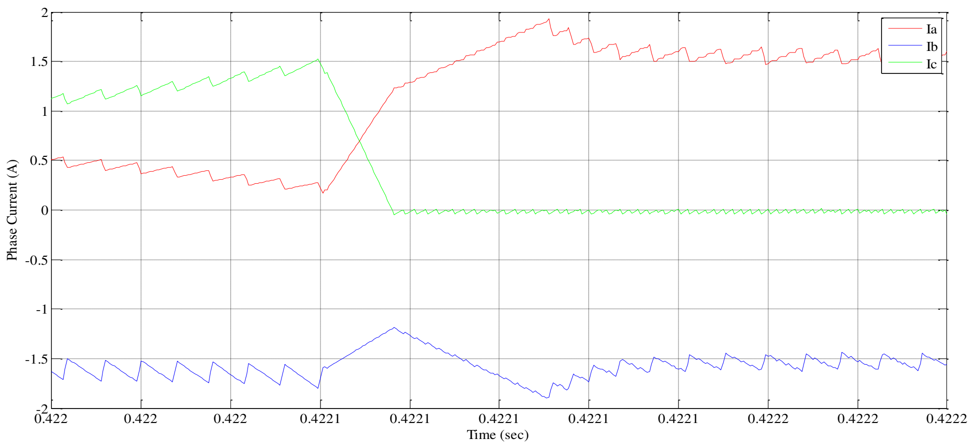

(c)

Fig. 4.18 Zoomed view of phase current at a speed of 2000 rpm (a) MTSDTC PWMON (b)MTSDTC ONPWM (c) TSDTC

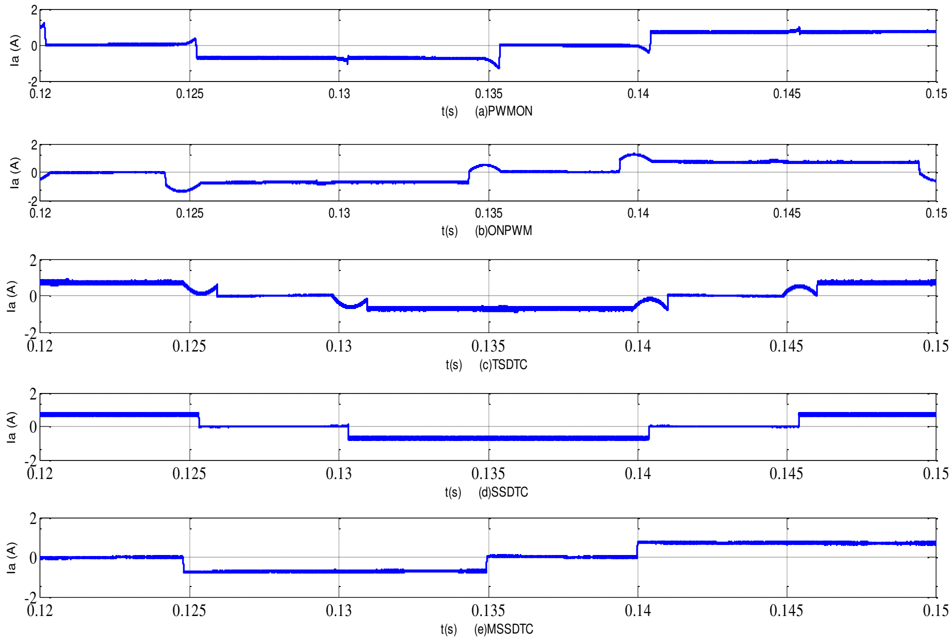

(a)

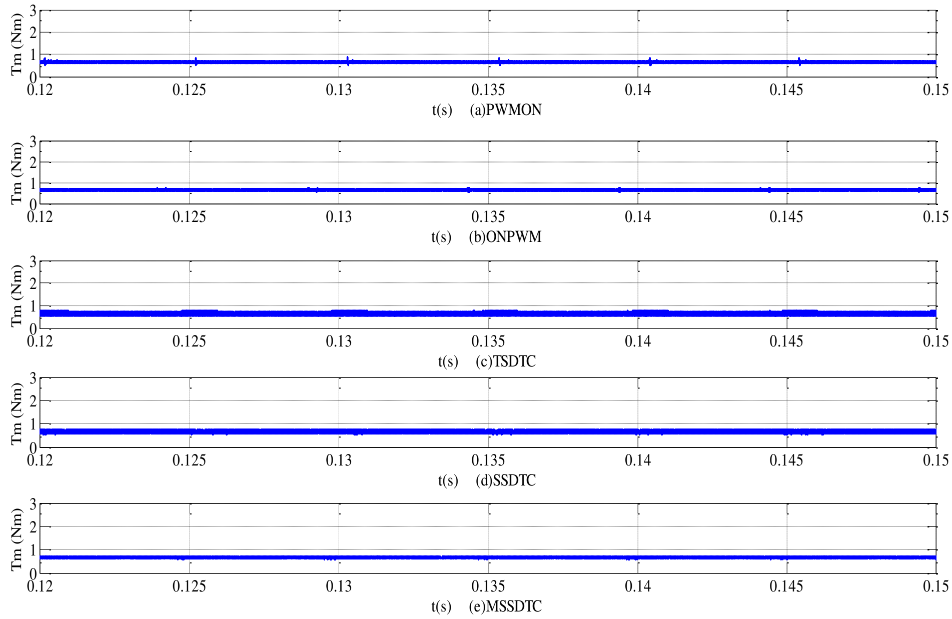

(b)

Fig. 4.19 Motor (a) phase current (b) torque ripple at a speed of 500 rpm for one cycle

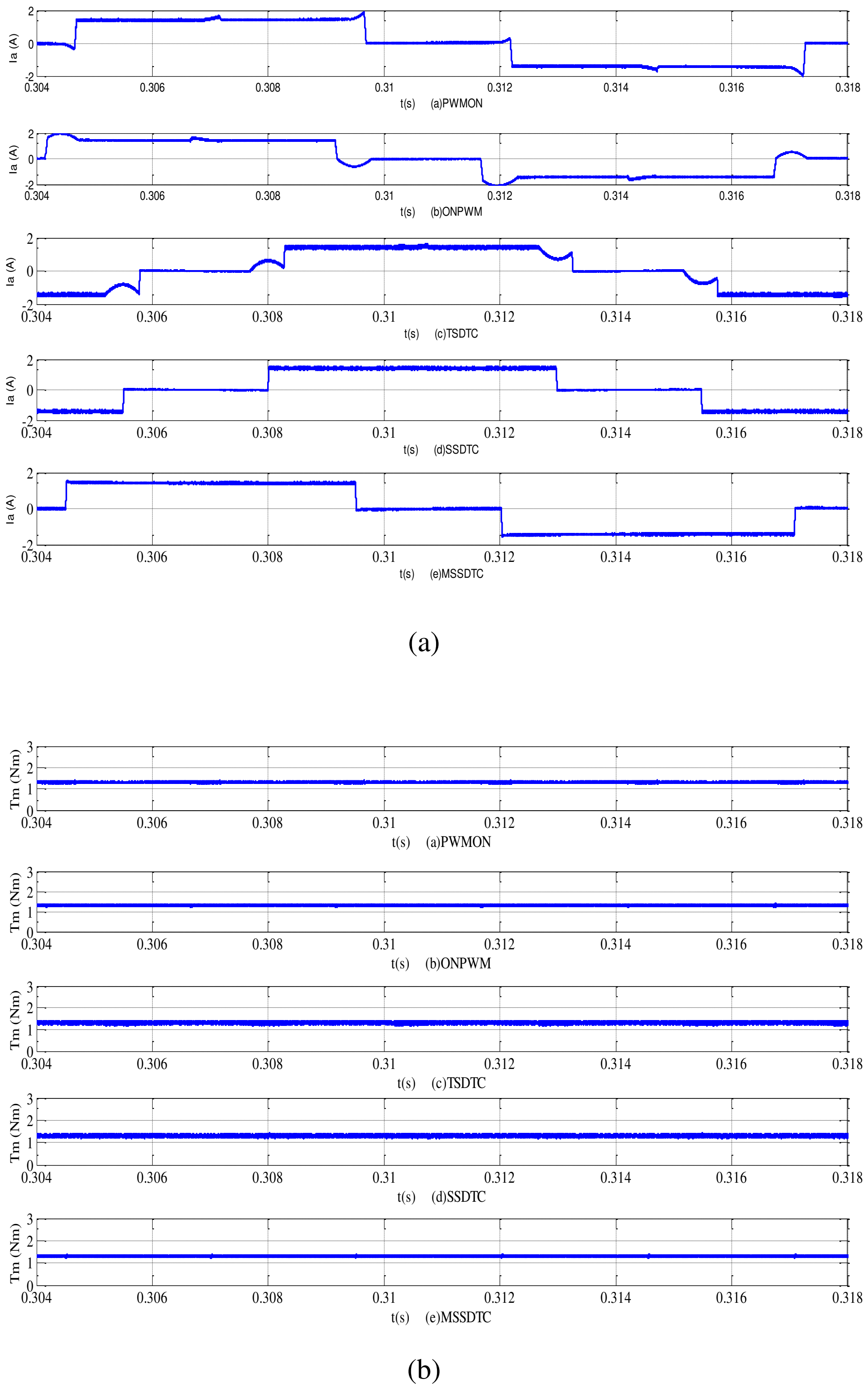

Fig. 4.20 Motor (a) phase current (b) torque ripple at a speed of 1000 rpm

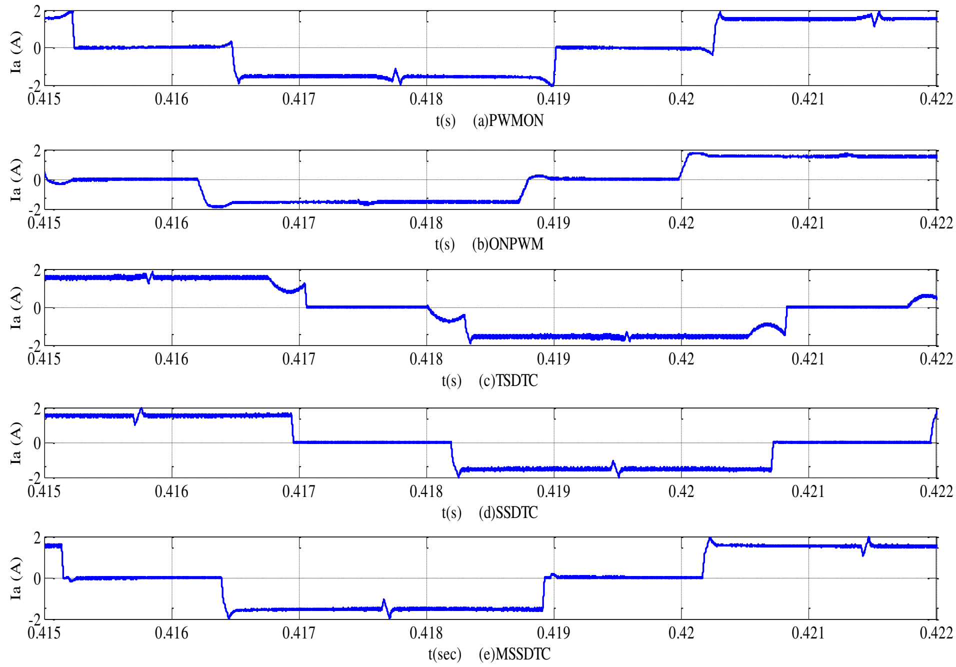

(a)

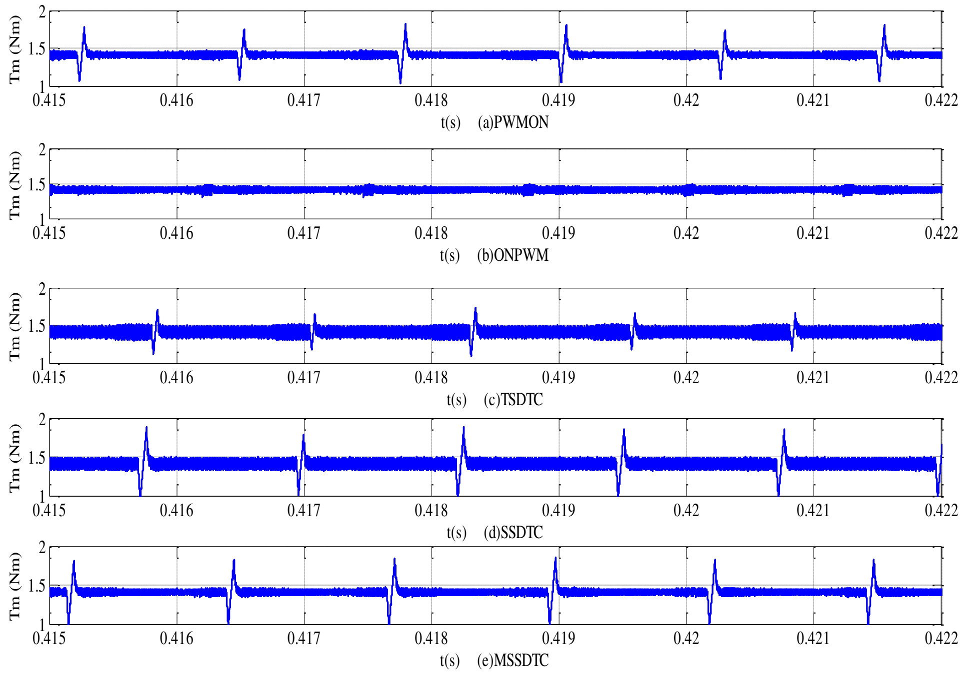

(b)

Fig. 4.21 Motor (a) phase current (b) torque ripple at a speed of 2000 rpm

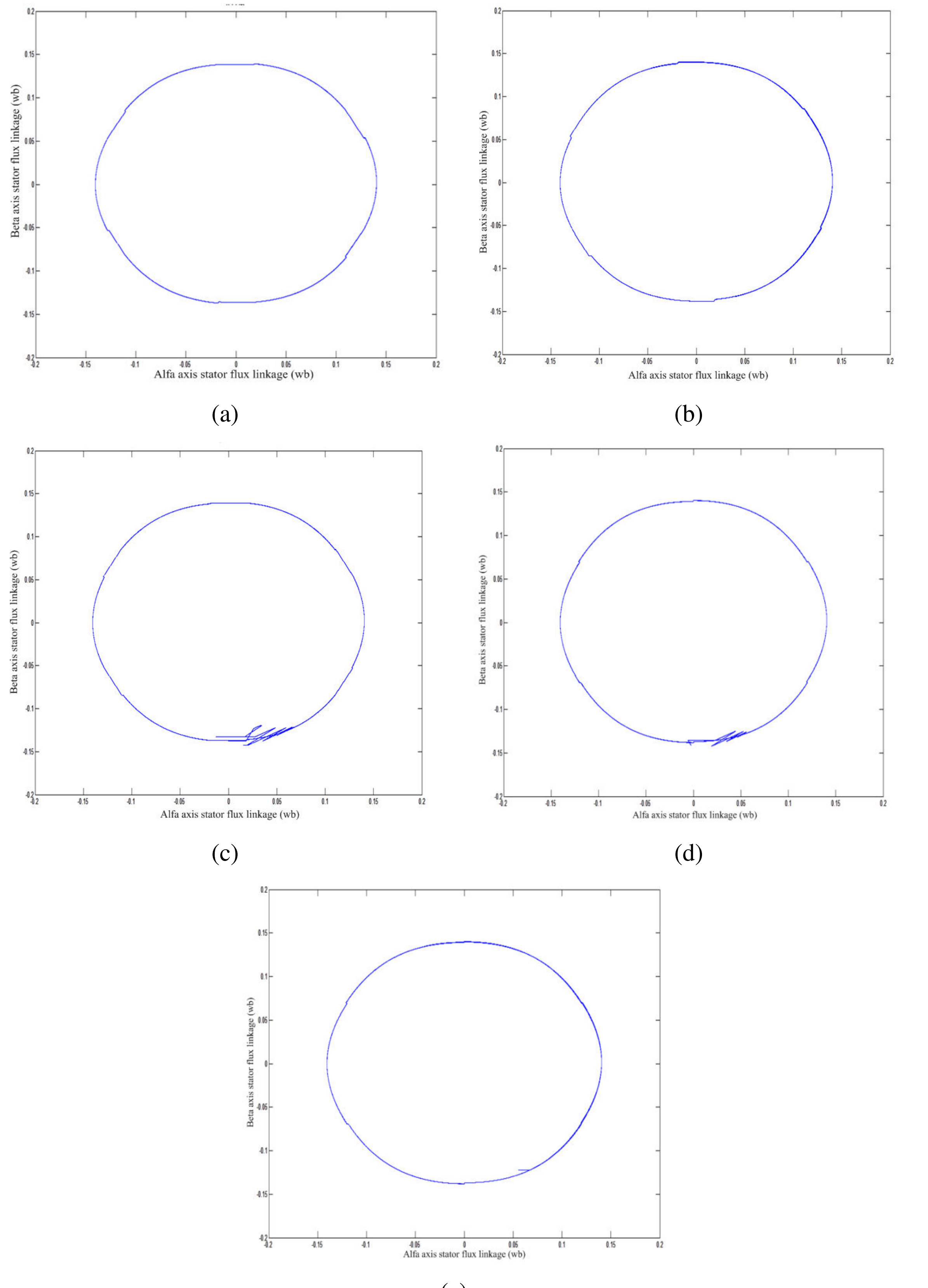

Fig. 4.22 Stator flux linkage plot for (a) MTSDTC PWMON (b) MTSDTC ONPWM (c) TSDTC (d) SSDTC (e) MSSDTC

4.4.1 Simulation result analysis of 2-3ΦO

Further to analyze the steady-state and dynamic performance of the BLDC motor with MTSDTC PWMON and ONPWM control with the TSDTC technique is provided in this section. More detailed simulation result analysis of the three techniques is discussed to show the effectiveness and comparison between the proposed techniques and conventional techniques with 2-3ΦO. The simulation is allowed to run for a period of 0.5s. The results provide the exact behavior of the BLDC motor drive parameters like gate pulses, theta, sector, motor torque, current, and speed with the conventional approach, and the two proposed methods. To analyze the steady-state and dynamic performance of the drive, the BLDC motor is allowed to run under constant load conditions at different speeds. The steady-state motor performance at a speed of 1000 rpm with an applied constant load of 0.5Nm for 2-3ΦO is as shown in Fig.4.23. The simulation results show that one electrical cycle is divided into 12 steps with the conduction and overlap region. The gating signals for the switch S1 and S2 with both the techniques justify the ONPWM and PWMON control. The motor reaches its set speed within 8ms for both techniques.

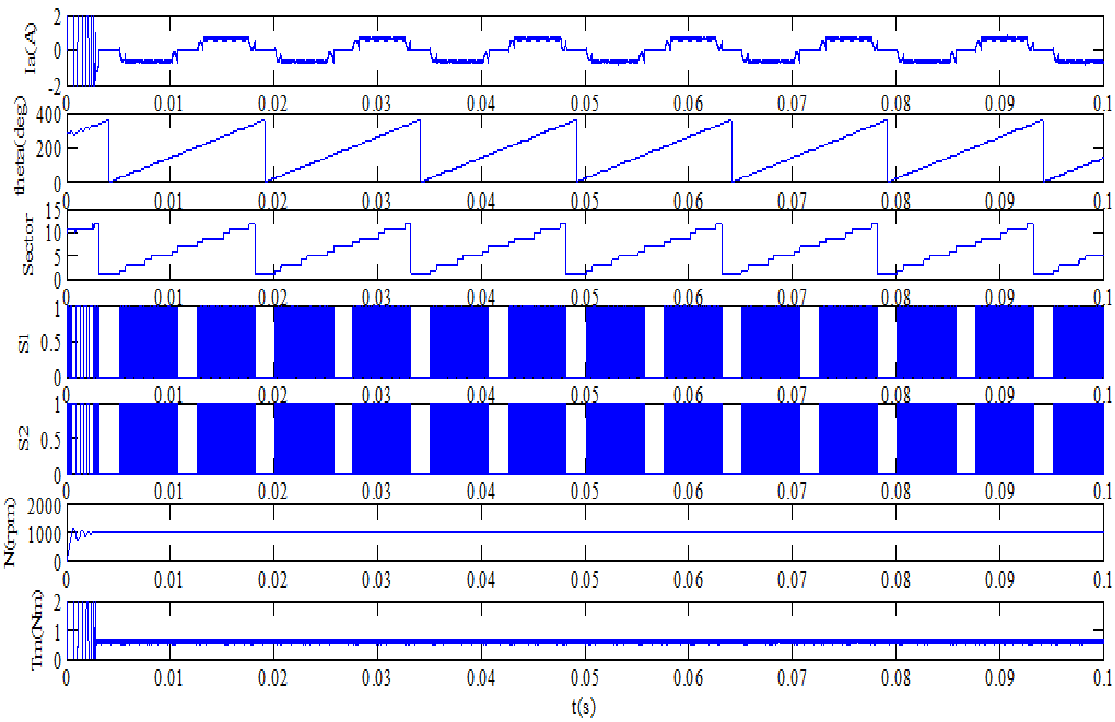

(a)

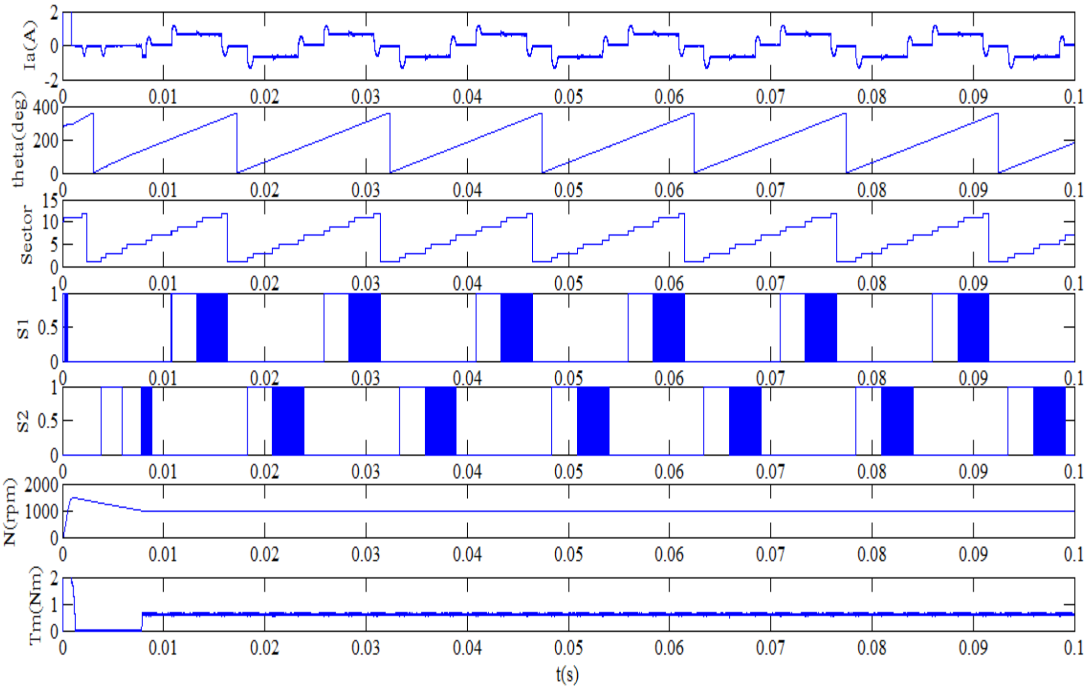

(b)

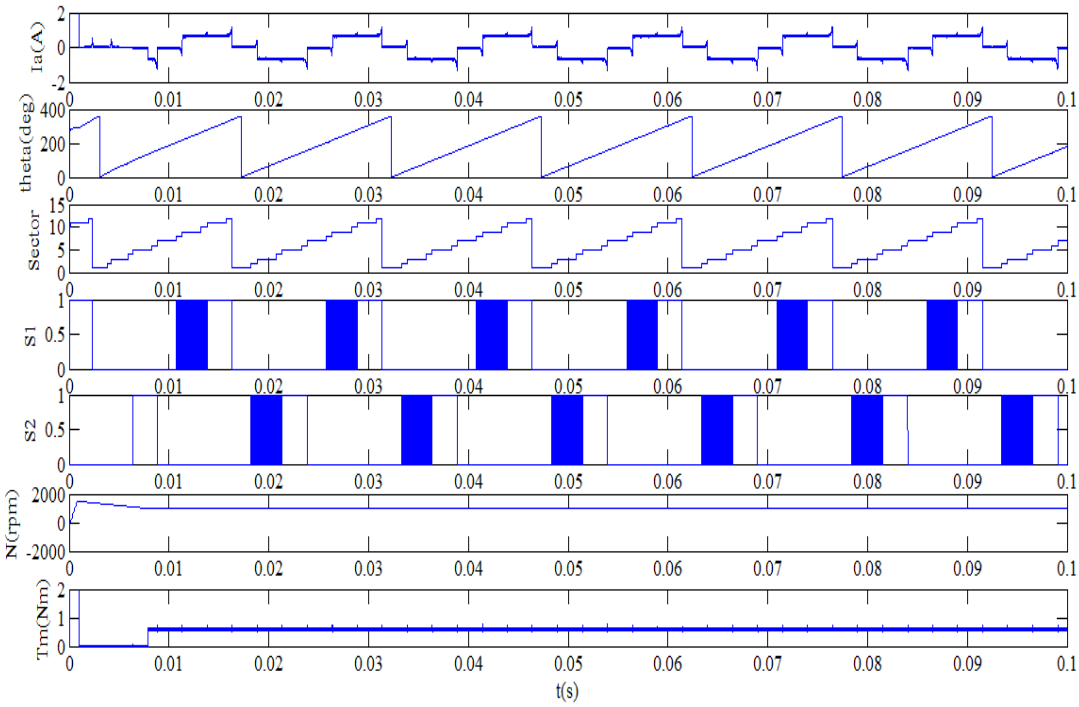

(c)

Fig. 4.23 Performance of BLDC motor drive at a speed of 1000rpm with a constant load of 0.5Nm with (a)TSDTC (b) ONPWM and (c) PWMON control

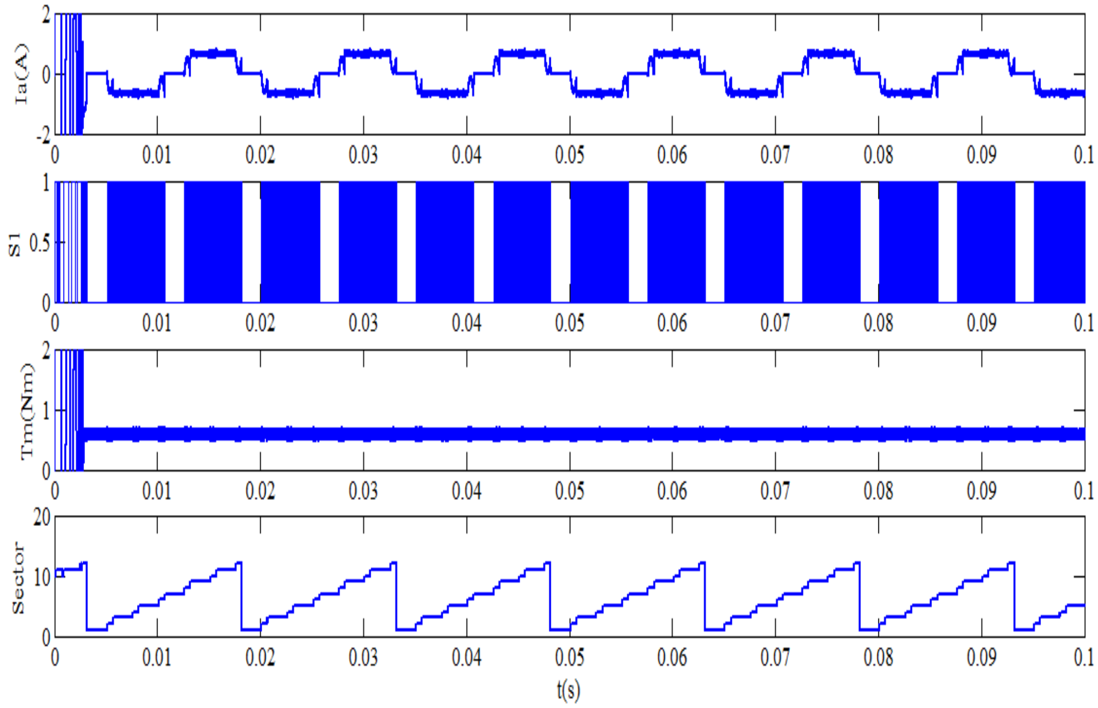

(a)

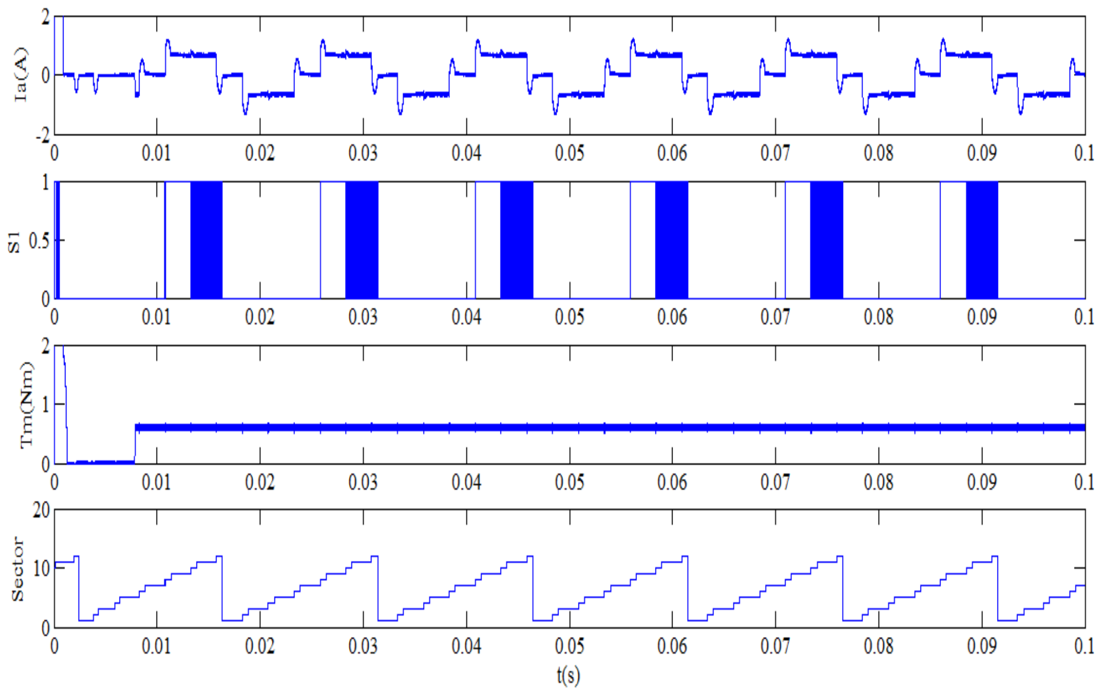

(b)

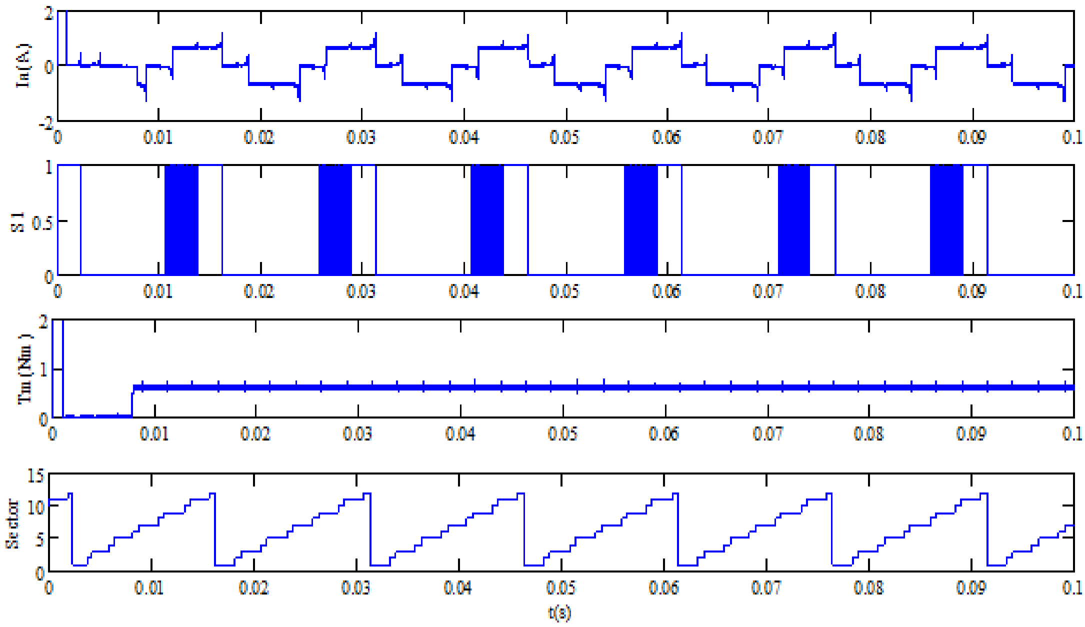

(c)

Fig. 4.24 Performance of BLDC motor with (a)TSDTC (b) ONPWM and (c) PWMON control with (i)phase current I_a (ii)gate pulse S1(iii)motor torque Tm and (iv) sector at speed of 1000 rpm with a constant load of 0.5Nm

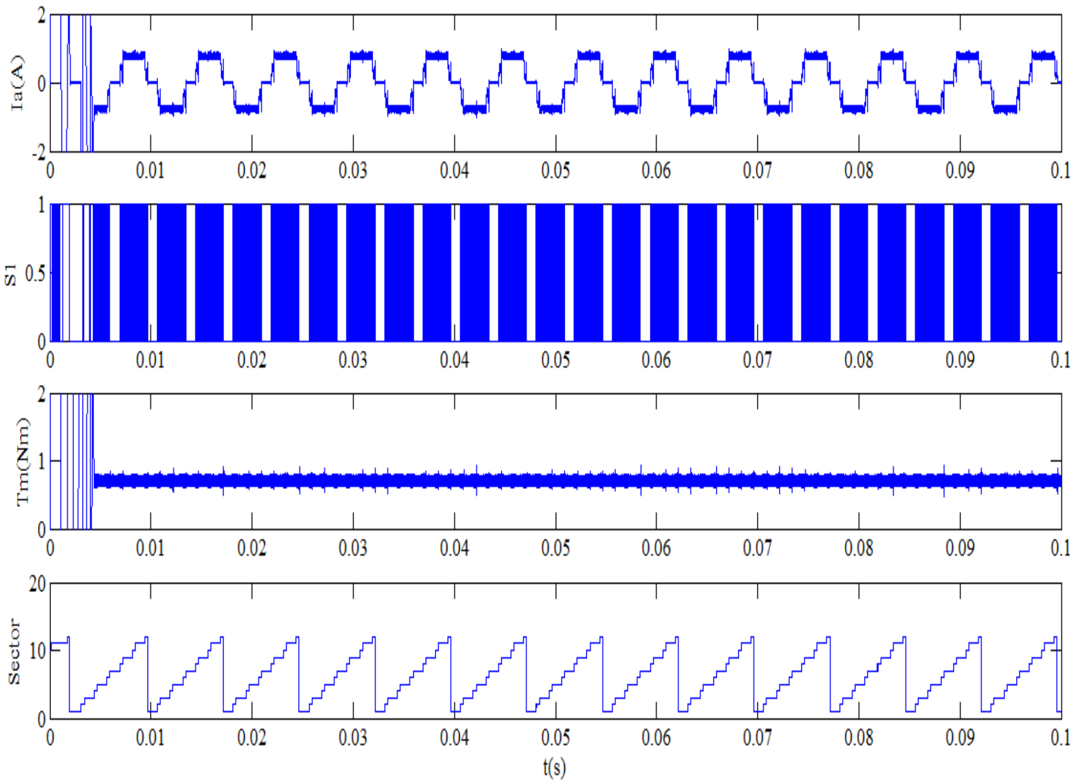

(a)

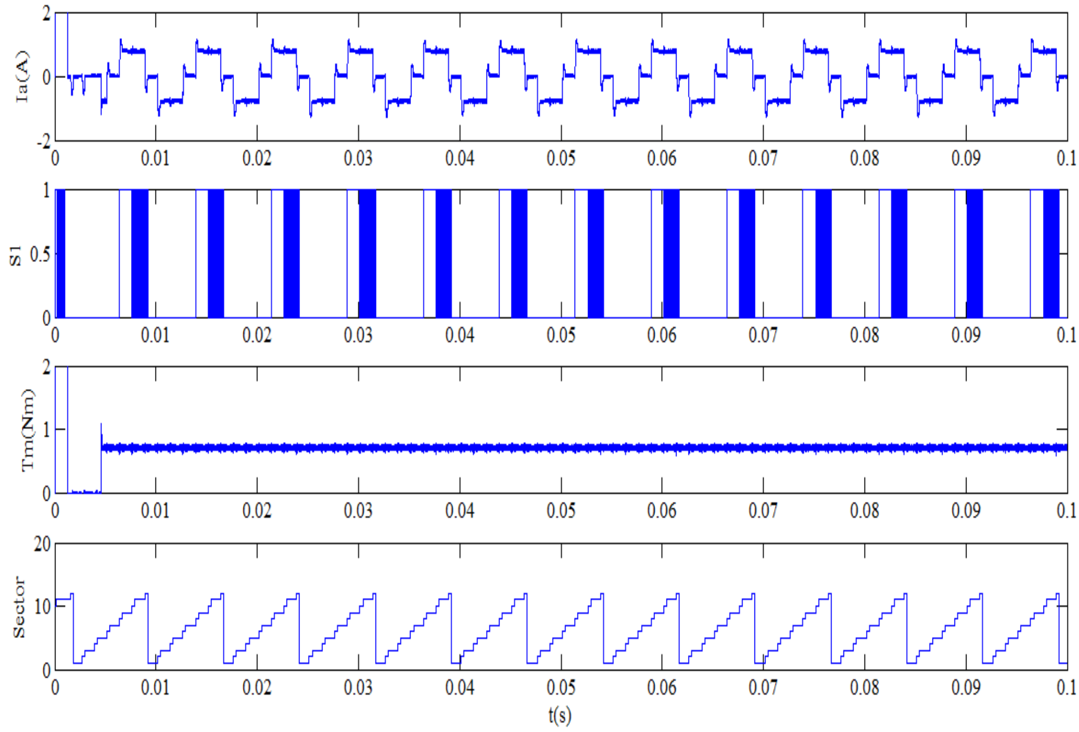

(b)

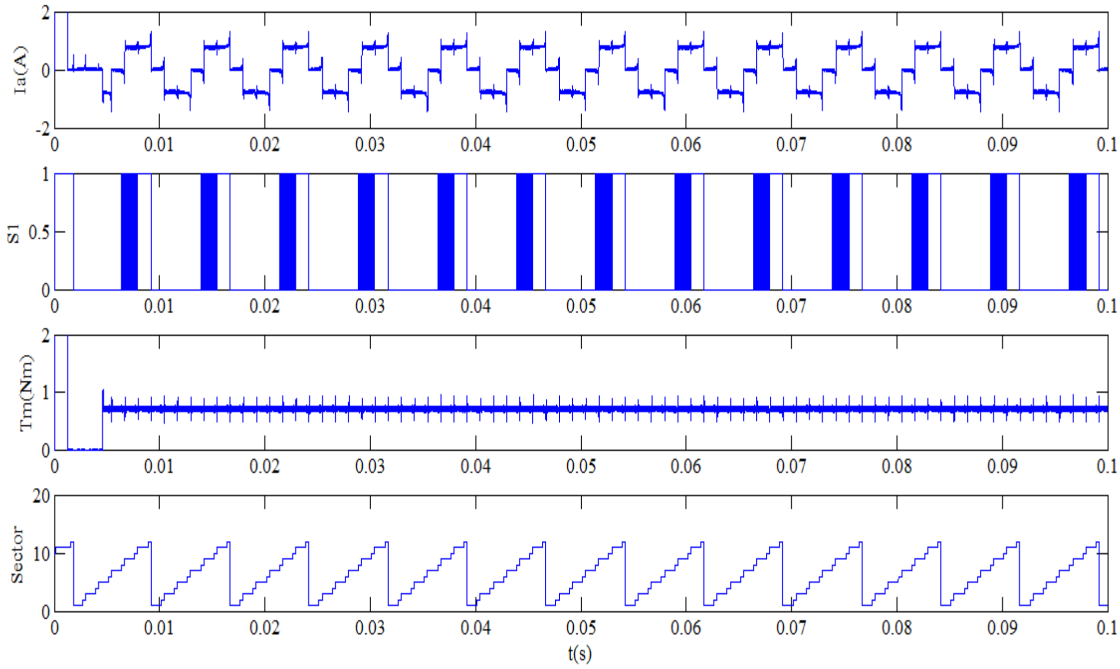

(c)

Fig. 4.25 Performance of BLDC motor with (a)TSDTC (b) ONPWM and (c) PWMON control with variation in (i)phase current I_a (ii)gate pulse S1(iii)motor torque Tm and (iv) sector at speed of 2000 rpm with a constant load of 0.5Nm.

The torque ripple at a speed of 1000rpm is slightly less with the ONPWM control than the PWMON control. The BLDC motor is allowed to run at a set speed of 1000rpm and 2000rpm with a constant load of 0.5Nm as shown in Fig.4.24 and Fig.4.25 respectively. The sector and voltage vector selection is done based on the lookup Table 4.4 and the computational logic Table 4.4 for TSDTC. For the ONPWM and PWMON control the inverter switches states are given in Table 4.7 and Table 4.8 respectively. The common computational logic for selecting the voltage vectors is as described in Table 4.6 to achieve the gate pulses as shown in Fig.4.24 and Fig.4.25.

The twelve steps for 2-3ΦO with the conventional and proposed technique are noticeable. When the motor torque is observed with all three techniques, the selection of the null vector with the MTSDTC ONPWM technique produces a reduced torque ripple as compared to the MTSDTC PWMON. Torque ripples in the conduction, as well as commutation region is high with the TSDTC technique as compared to the proposed techniques. Now comparing the two proposed techniques, the torque ripple increases with the MTSDTC PWMON technique with the set speed of 2000 rpm. The dynamic motor performance comparison for the 2-3ΦO is as shown in Fig.4.26. The time taken by the controller to reach the set speed is very less. There is a smooth speed change from 1000rpm to 2000rpm at 0.2s but the controller takes some finite time to decrease the speed to 1000rpm at 0.4s for the proposed techniques but small oscillations are observed with the conventional techniques.

It can be depicted that the motor oscillates to settle at the set speed during starting and with an increase in reference speed. It can be concluded that the proposed MTSDTC ONPWM method gives better speed control with reduced steady-state error and oscillations at all higher speeds with the same PI controller. The selection of suitable voltage vectors from the lookup tables for the proposed techniques has made it possible to reduce the switching losses and the commutation torque ripple with the proposed technique. The ripple in torque in the commutation region is high with the conventional TSDTC and proposed MTSDTC PWMON as compared to the MTSDTC ONPWM technique at low speed and it is almost eliminated with the proposed MTSDTC ONPWM technique at higher speed.

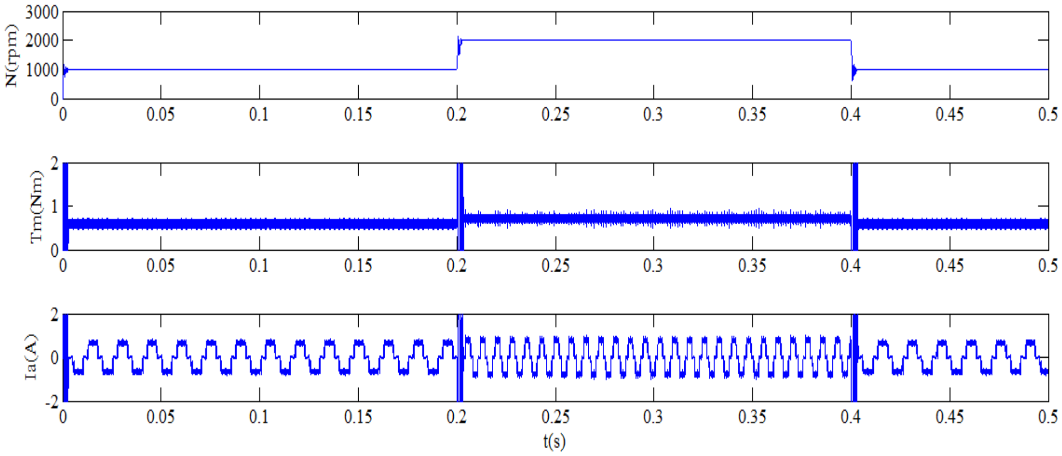

(a)

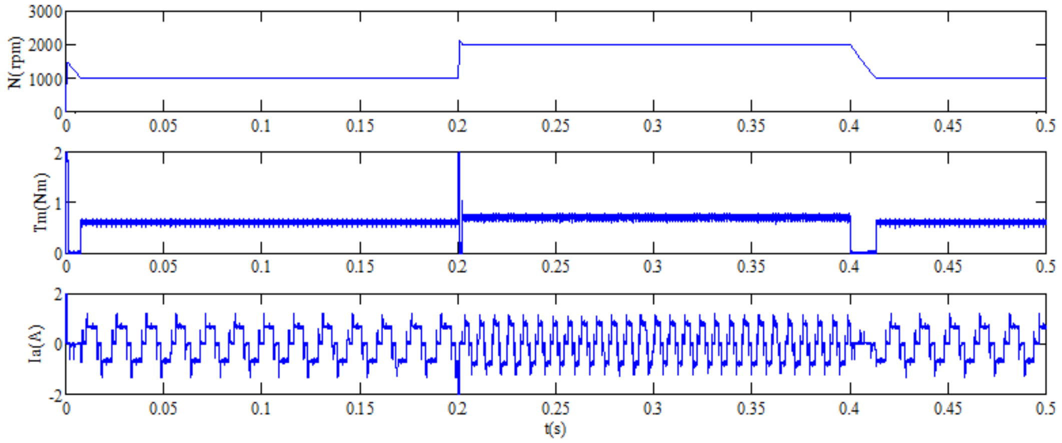

(b)

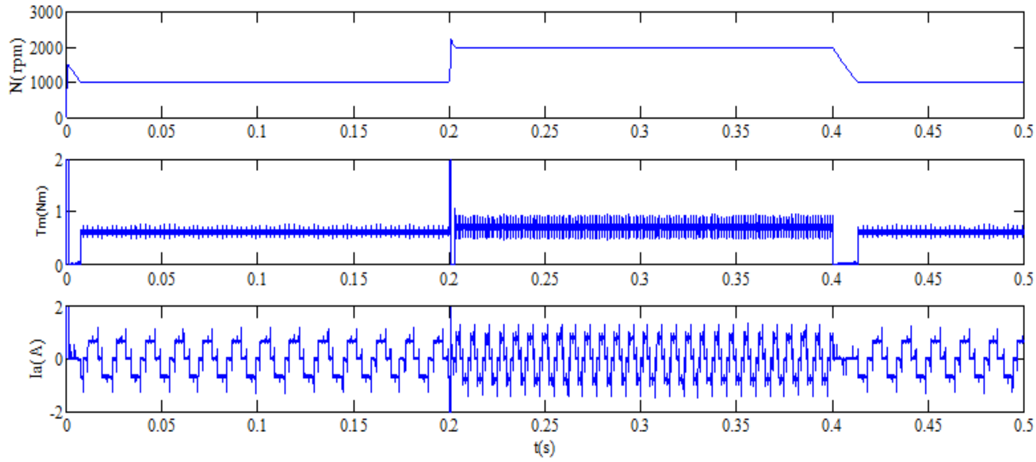

(c)

Fig.4.26 Dynamic motor performance comparison with an applied speed change at 0.2s and 0.4s with a constant load of 0.5Nm showing variation in (i)speed (ii) motor torque (iii) phase current for variable speed operation between (a)TSDTC (b)proposed MTSDTC ONPWM and (b) proposed MTSDTCPWMON

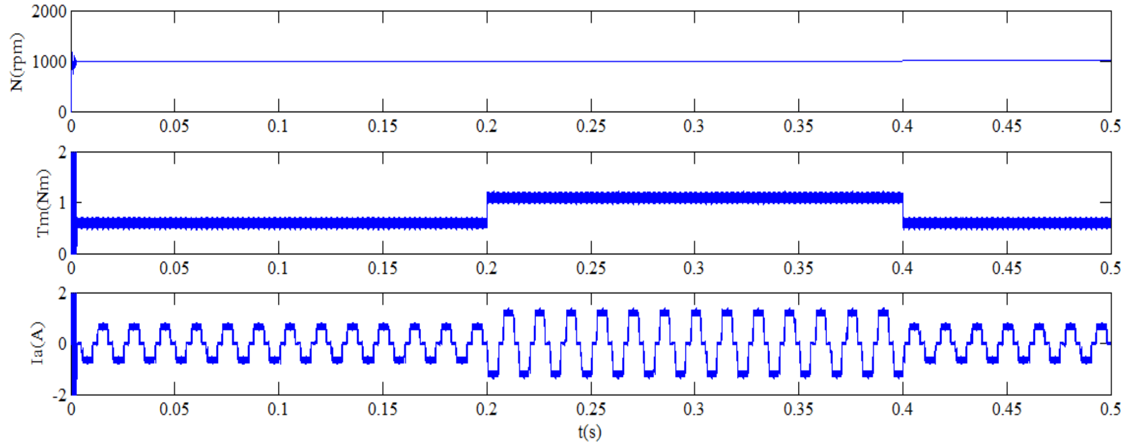

(a)

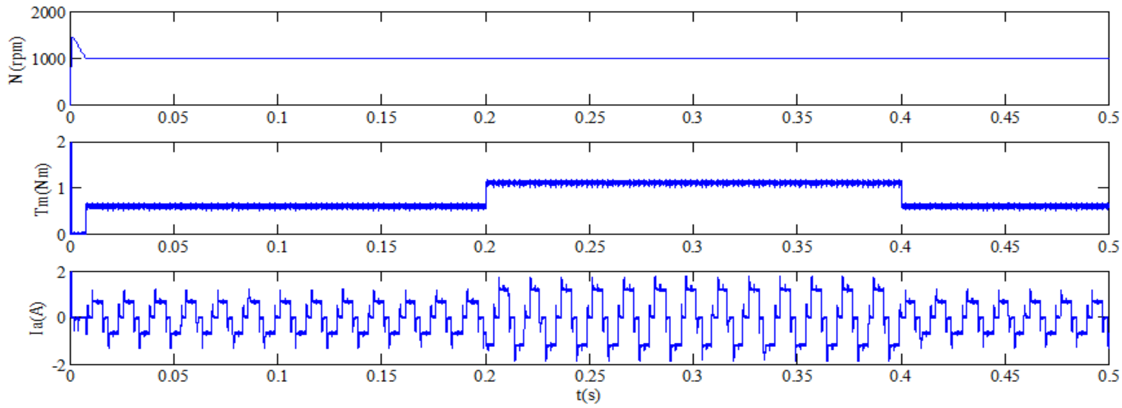

(b)

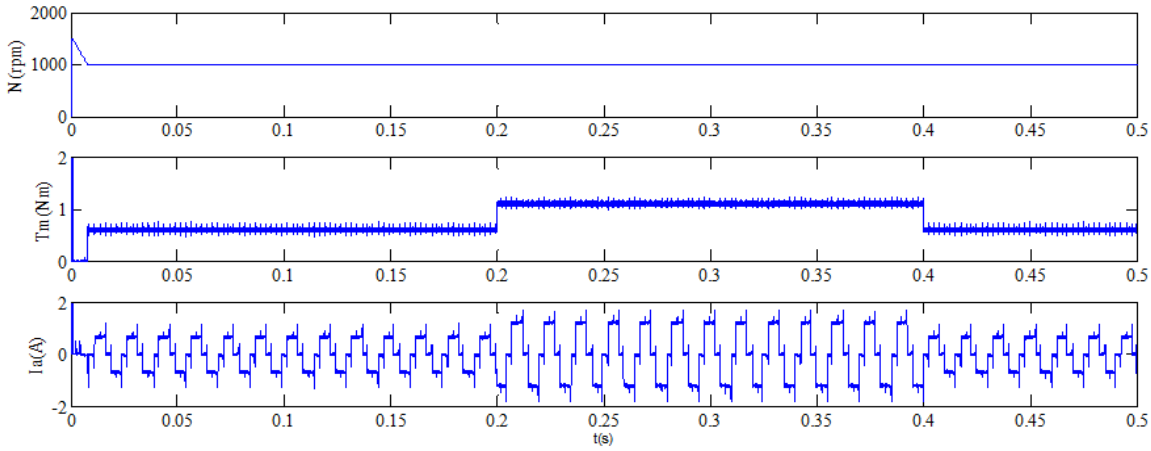

(c)

Fig.4.27 Dynamic motor performance comparison with a set speed of 1000rpm and applied load changes at 0.2s and 0.4s between showing variation in (i)speed (ii) motor torque (iii) phase current between (a)TSDTC (b)proposed MTSDTC ONPWM and (b) proposed MTSDTC PWMON

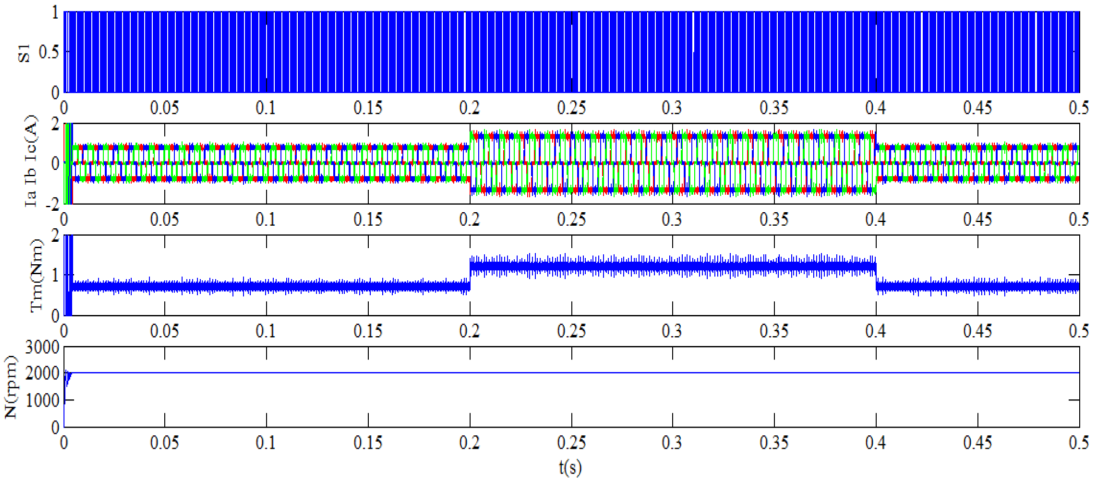

(a)

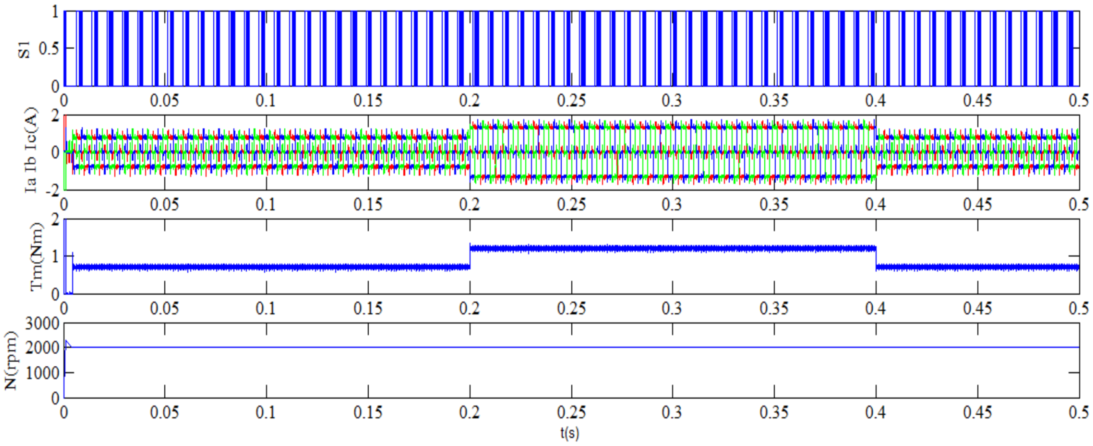

(b)

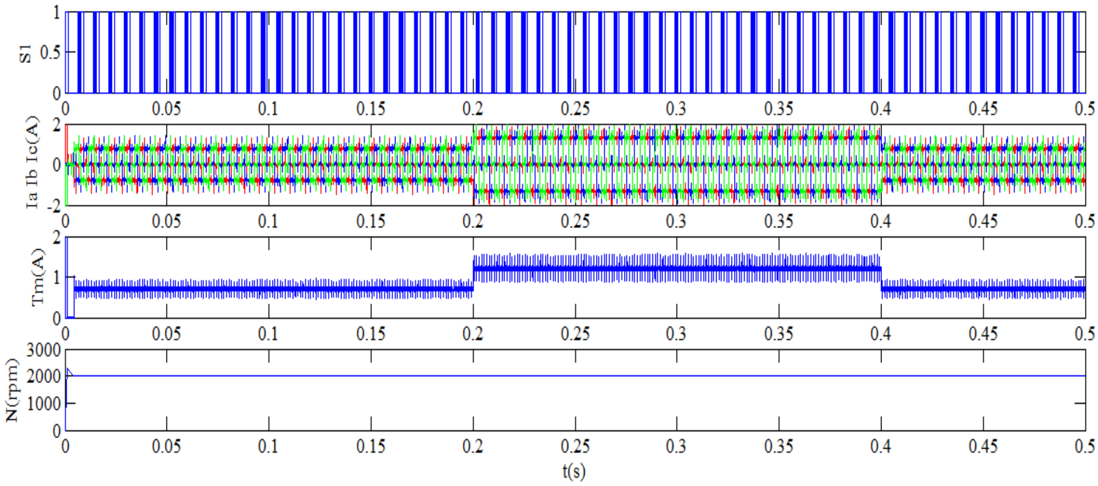

(c)

Fig.4.28 Dynamic motor performance comparison with applied load changes at 0.2s and 0.4s with a set speed of 2000 rpm showing variation in (i)gate pulses (ii)three-phase current (iii) motor torque (iv) speed between (a)TSDTC (b)proposed MTSDTC ONPWM and (c) proposed MTSDTC PWMON

The motor dynamic performance is checked with fixed speed and variable load conditions. The motor is operated at a speed of 1000 rpm with the load varying from 0.5Nm to 1Nm at 0.2s and then reduced to 0.5Nm at 0.4s as shown in Fig.4.27. The magnitude of the stator phase current increases as the load increases with the reference speed set to 1000 rpm. The PI controller takes around 9ms to reach the set speed. Again it can be observed that the ripple in torque in the commutation region is high with the conventional TSDTC and the proposed MTSDTC PWMON at a higher speed as compared to the MTSDTC ONPWM technique and is almost eliminated with the ONPWM control which results in the smooth operation of BLDC drive. The dynamic performance of the motor is also performed with applied load changes at 0.2s and 0.4s with a set speed of 2000 rpm as shown in Fig.4.28. It can be observed that the torque ripple is reduced with the proposed ONPWM control under varied load conditions and higher speeds. Some oscillations are observed in the speed during the starting with the conventional TSDTC and overshoot with the proposed methods but the effective tuning of the PI controller takes less than 5ms to reach its steady-state.

By comparing the DTC techniques for 2-3ΦO, the ripple in torque in the commutation region is high for the proposed MTSDTC PWMON as compared to the TSDTC technique but, it is almost eliminated with the proposed MTSDTC ONPWM technique which results in the smooth operation of BLDC drive.

4.5 **Experimental results**

The simulation results of the proposed MTSDTC techniques with ONPWM and PWMON control are validated by the experimental results produced under different speed and loading conditions. The schematic block diagram of the overall system required for the hardware implementation is as shown in Fig.4.29. The hardware implementation is carried on the same experimental setup as shown in Fig. 3.11. The experimental setup consists of a 36 volt, 4 pole BLDC motor with a belt and pulley type loading arrangement. The closed-loop control of the drive using the proposed technique is implemented with STM32F407VG ARM controller discovery card having a clock frequency of 168 MHz, a three-phase voltage source inverter (VSI) card with six insulated gate bipolar transistors (IGBTs), current and voltage sensor cards, a driver card for isolating the power circuit from the control circuit and DC power supply for the inverter card, driver card, and the controller.

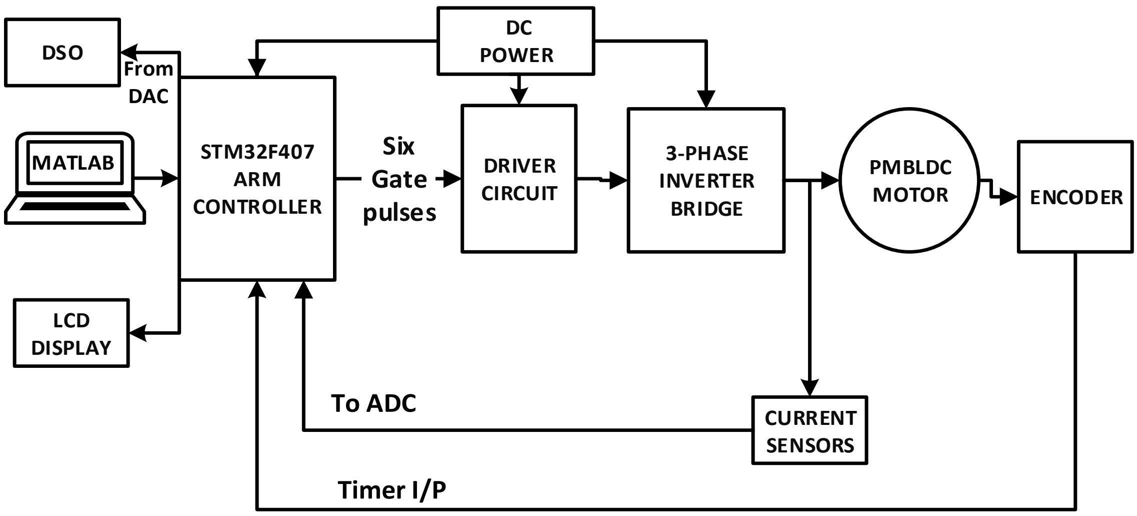

Fig.4.29 Schematic block diagram of the overall system

An advanced Timer-8 is utilized to generate the six gate pulses for six inverter switches. The reference speed and the actual speed are displayed on the LCD. The value of switching frequency is 10 kHz, the sampling frequency of inner loop quantities is 25 kHz and the outer speed loop operates at 2.5 kHz. The hardware results are captured using 4channel Digital Signal Oscilloscope. The speed control loop is incorporated using a PI controller to process the error signal generated from the comparison between the reference speed and actual speed. The output of the 1250 ppr inbuilt shaft encoder is used to calculate the speed is given to the A9 and E9 pin of timer 1 of the controller card. A shift in speed from 1000rpm to 2000rpm and then from 2000rpm to 1000rpm is applied to witness the motor behaviour under constant load conditions. The BLDC motor performance is also tested by varying the load under constant speed conditions. The accurate tuning of the PI controller allows the motor speed under closed-loop control to follow the reference speed. A belt and pulley arrangement is provided for loading the motor. A maximum loading of up to 2.5 ampere can be provided for the given motor. The loading is provided by increasing the tension on the belt. The experimental results of the BLDC motor drive prove the effectiveness of the proposed technique by validating the simulation results in real-time.

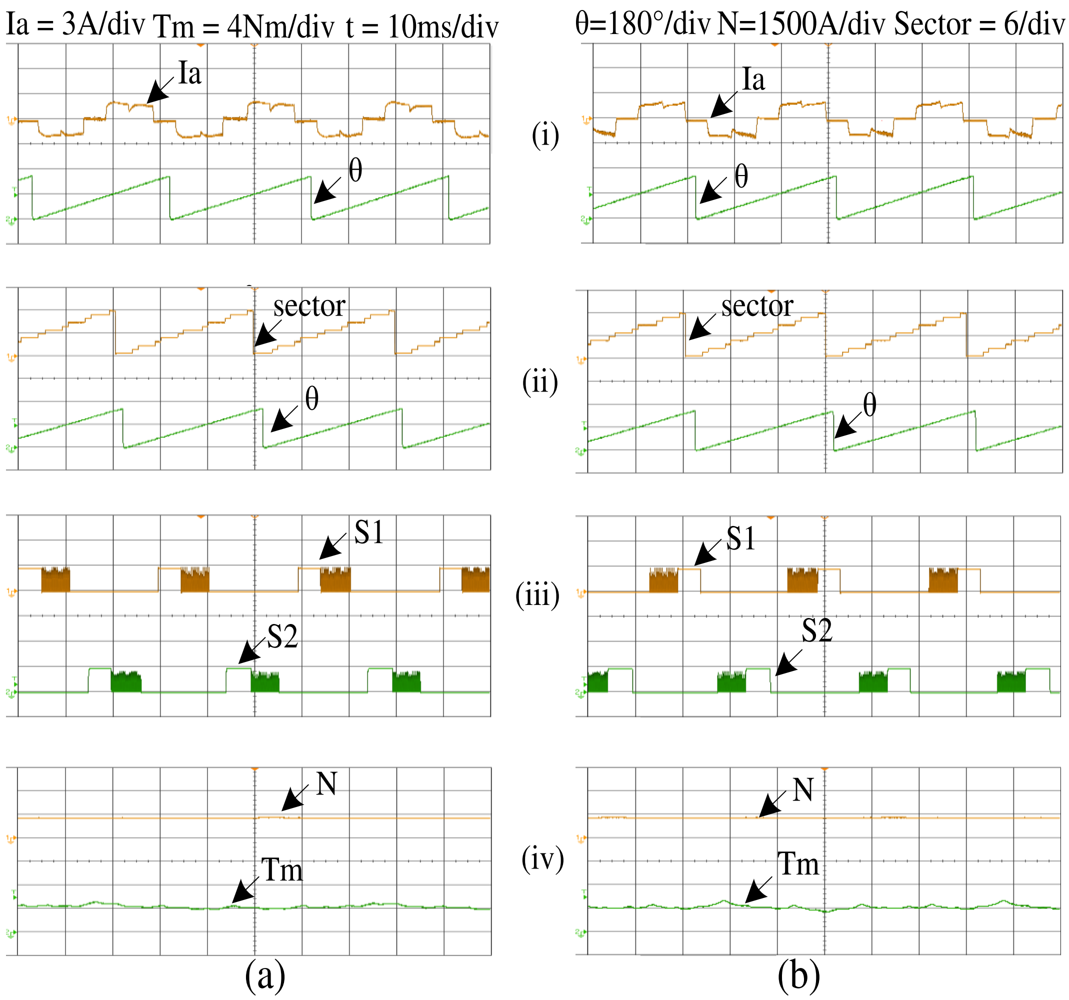

Fig. 4.30 Steady-state performance of BLDC motor (i) current and theta (ii) sector and theta (iii) gating pulse for switch S1 and S2 (iv) speed and torque at a speed of 1000 rpm with an applied load of 2A for proposed (a) MTSDTC ONPWM and (b) MTSDTC PWMON

The proposed modified twelve-step DTC technique with a fixed 15° overlap region provides twelve steps with 2-3ΦO in one electrical cycle as shown in Fig.4.30 to Fig.4.32 for motor operation at different speeds and loading condition to attenuate the commutation torque ripple. As shown in Fig. 4.30, with the proper selection of voltage vectors and null vectors for the proposed techniques MTSDTC ONPWM and MTSDTC PWMON from the lookup Table 4.7 and Table 4.8 based on the computational logic Table 4.6. generates the required gate pulses for the switches S1 and S2 of the same phase leg such that the requirement of the dead band is eliminated which increases the reliability of the drive.

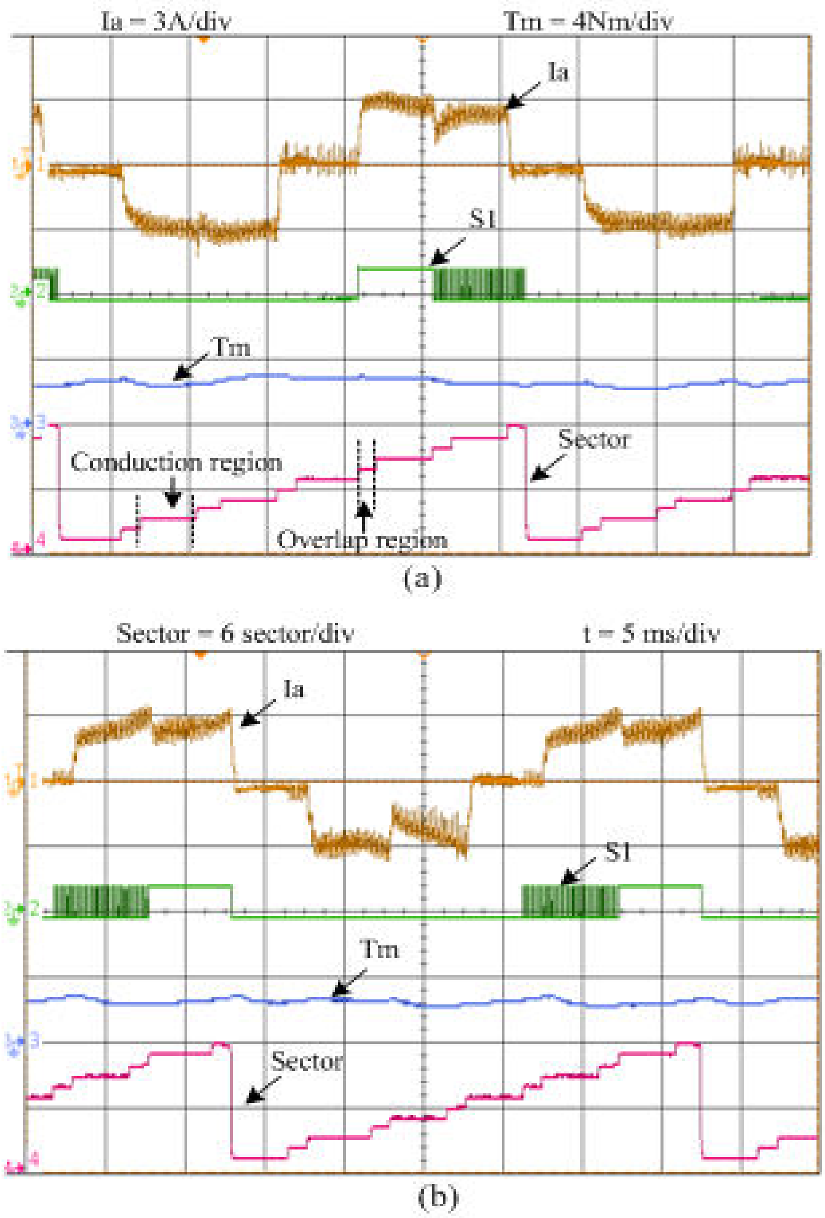

Fig. 4.31 Steady-state performance of motor with proposed DTC technique at a speed of 1000 rpm with an applied load of 2A for (a) MTSDTC ONPWM and (b) MTSDTC PWMON

The results shown in Fig.4.31 and Fig.4.32 provide the steady-state performance of the BLDC motor drive at a speed of 1000rpm and 2000rpm with a constant load of 2A respectively for both the proposed methods. The twelve step operation is clearly distinguished with the six sectors and six overlap regions. The inverter switching with the

MTSDTC ONPWM and PWMON control is justified in the results. At a speed of 2000 rpm the torque ripple are less with the ONPWM technique. The quasi square wave current provides dip notches with the PWMON technique resulting in higher torque ripple.

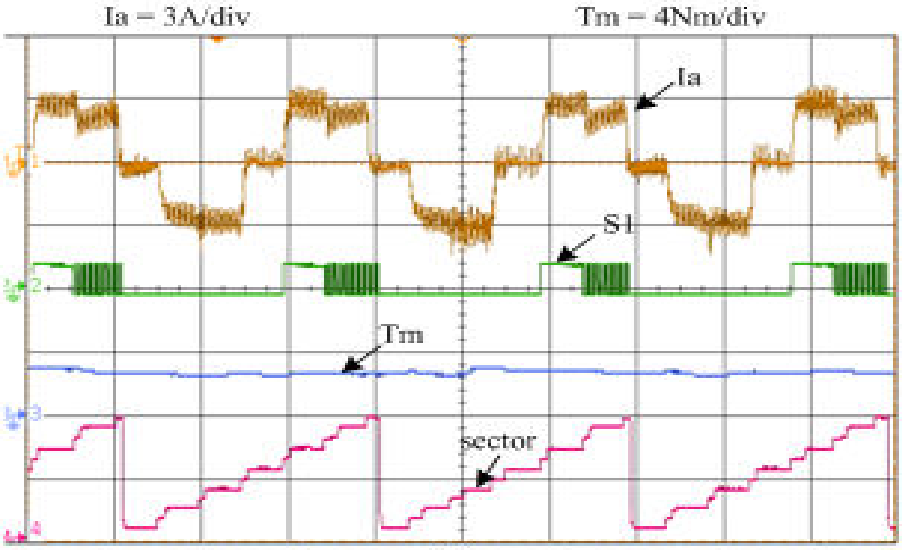

(a)

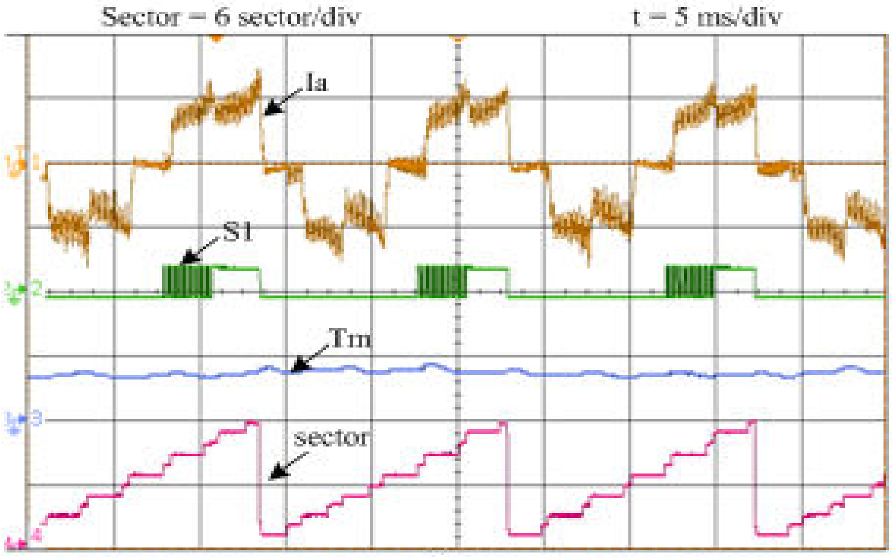

(b)

Fig. 4.32 Steady-state performance of motor with proposed DTC technique at a speed of 2000 rpm with an applied load of 2A for (a) MTSDTC ONPWM and (b) MTSDTC PWMON

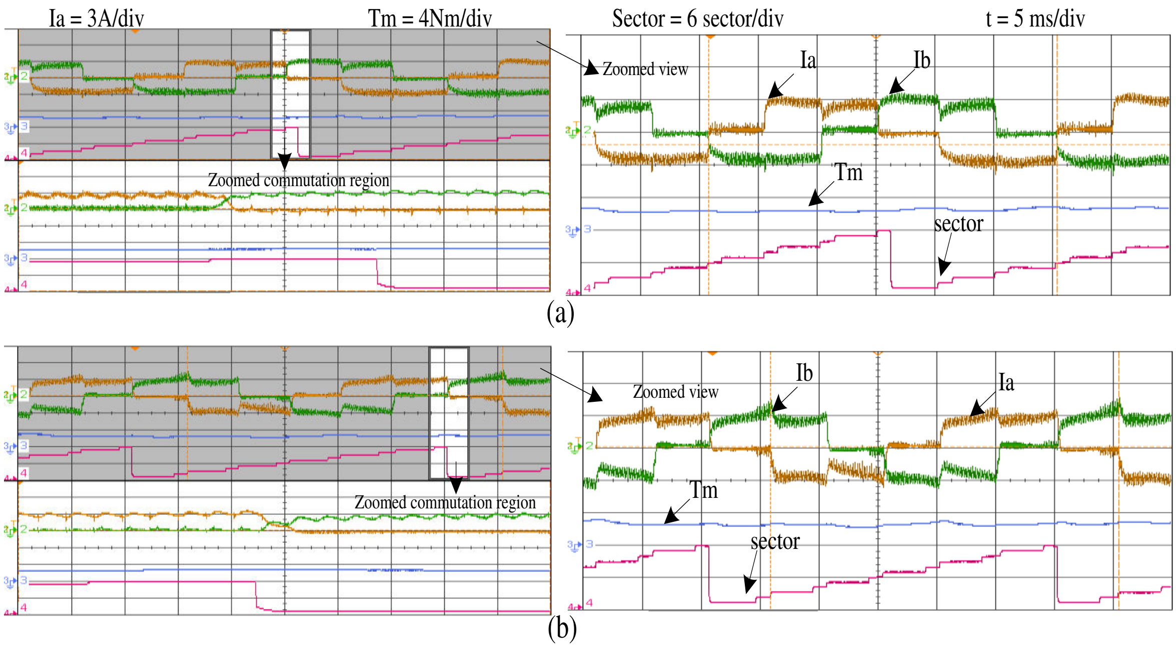

Fig. 4.33 Behavior of BLDC motor current and torque in the conduction and commutation region with under steady-state at a speed of 2000rpm with an applied load of 2A for the proposed (a) MTSDTC ONPWM (b) MTSDTC PWMON

It can be observed that the conduction time with the MTSDTC ONPWM is 11ms and 5ms at a speed of 1000 rpm and 2000rpm respectively with a constant load of 2A.Under the same operating condition, the conduction time with MTSDTC PWMON method is 13ms and 6ms. The magnitude of the motor current remains constant as the load is constant. The behavior of motor torque in the commutation region at a speed of 1000 rpm with a constant load of 2A is observed in Fig. 4.33. The zoomed view provides better resolution of the waveforms. With almost the same rate of change of current between the outgoing and incoming current, the smooth motor torque is obtained with the proposed technique MTSDTC ONPWM as compared to the PWMON technique.

The waveforms of current, switching signals, and theta showing the twelve step operation justifies the simulation results for both the techniques validating the proposed approach. The motor operation under varied speed and load condition and its detailed analysis is provided in the results shown in Fig.3.34 to Fig. 4.36.

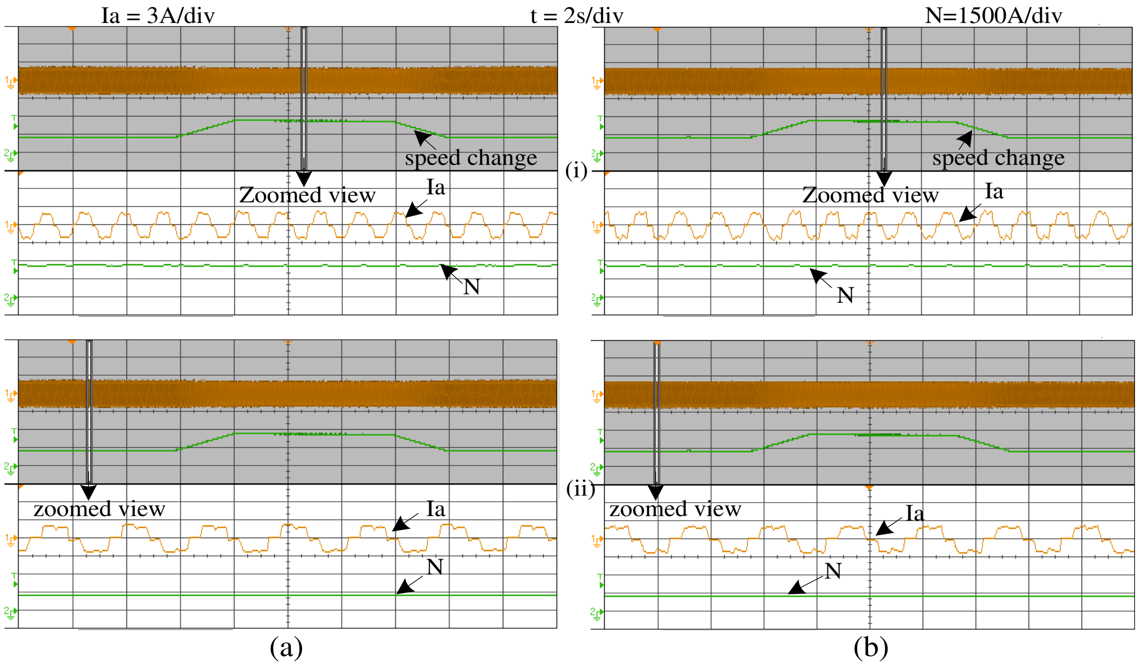

Fig. 4.34 Dynamic performance of BLDC motor with speed change from 1000rpm to 2000rpm and from 2000rpm to 1000 rpm (i) zoomed view of current and speed at 2000rpm (ii)) zoomed view of current and speed at 1000rpm with a constant applied load of 2A for the proposed(a) MTSDTC ONPWM (b) MTSDTC PWMON

The comparison of the dynamic performance of the motor drive for both the proposed methods is obtained in Fig.4.34 with the applied speed change from 1000rpm to 2000rpm with an applied constant load of 2A. It can be observed that the magnitude of the phase current remains constant with the change in speed. The fine-tuned PI controller takes around 2s to reach the set speed of 2000 rpm from 1000rpm with sudden applied speed change.

The motor operation under varying load conditions at a speed of 1000 rpm is shown in Fig.4.35. With sudden applied load change, the variation in the magnitude of the phase current can be observed with the speed remaining almost constant with a small dip at the time of load change. The magnitude of the current increases with the increase in load to meet the torque demand. From Fig.4.36 it is observed that with the applied load change the motor torque changes with the speed remaining constant at a set speed of 1000rpm. As load is increased, the motor torque increases as the magnitude of current increases. A small rising dip in the speed is observed in Fig.4.36(a) when the load is reduced with the MTSDTC ONPWM and for MTSDTC PWMON shown in Fig.4.36(b), dips are spotted during the rise and fall in load. The fine-tuning of the PI controller allows the motor to follow the set speed under different loading conditions.

From the simulation results, a comparative analysis is provided in Table 4.9 to compare the effectiveness of the proposed MTSDTC PWMON and ONPWM control with the other DTC technique under 2-ΦO and 2-3ΦO.

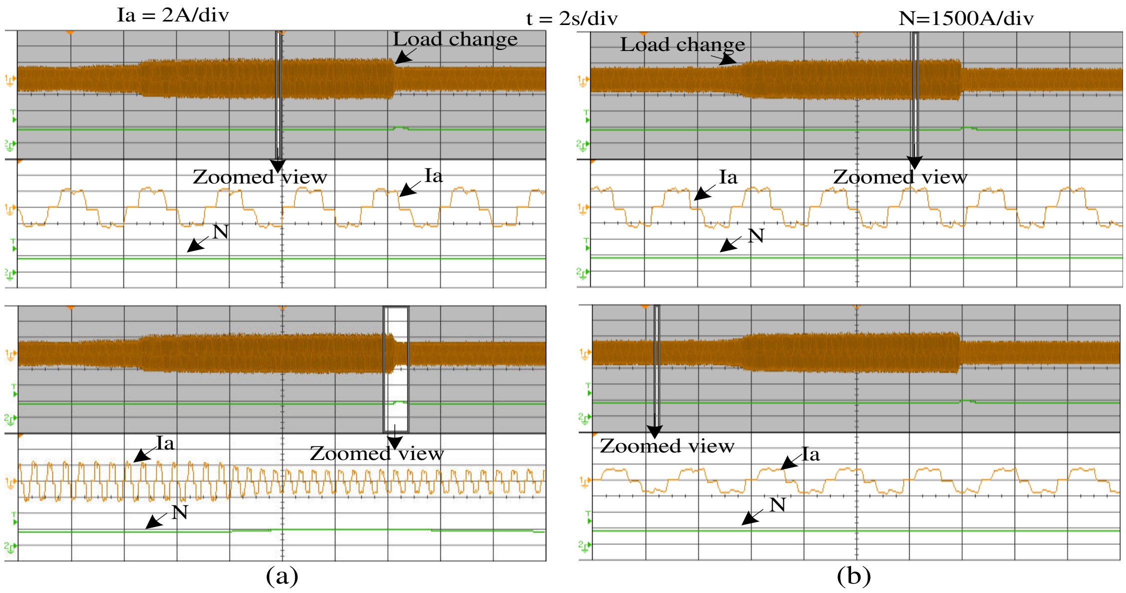

Fig. 4.35 Dynamic performance of BLDC motor with a constant speed of 1000rpm under applied load change condition for the proposed(a) MTSDTC ONPWMand (b) MTSDTC PWMON

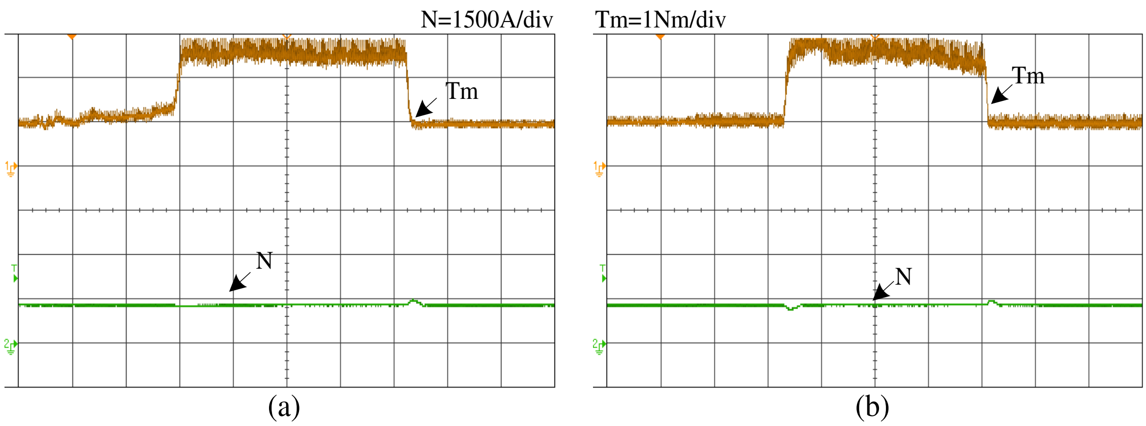

Fig. 4.36 Dynamic performance of BLDC motor with applied load change and constant speed of 1000 rpm for the proposed(a) MTSDTC ONPWM and (b) MTSDTC PWMON

Table 4.9 Comparative analysis of proposed MTSDTC PWMON, MTSDTC ONPWM TSDTC, SSDTC, and MSSDTC technique

DTC Techniques	**Speed(rpm)**	**Load (Nm)**	**% Comm. Torque ripple**
MTSDTC PWMON	500	0.6	46.15
	1000	1.2	16.91
	2000	1.2	43.97
MTSDTC ONPWM	500	0.6	15.38
	1000	1.2	10.76
	2000	1.2	12.27
TSDTC	500	0.6	30.75
	1000	1.2	16.92
	2000	1.2	39.43
SSDTC	500	0.6	25
	1000	1.2	14.67
	2000	1.2	85.71
MSSDTC	500	0.6	8.39
	1000	1.2	10.93
	2000	1.2	64.28

The comparative analysis plot reflecting the % commutation torque ripple for different DTC technique at different speed and loading condition is shown in Fig. 4.37. It is plotted from the data provided in Table 4.9. It shows that the commutation torque ripple is less with the MSSDTC technique at low speed and high speed with 2-ΦO as compared to the conventional SSDTC. Among the three techniques for 2-3ΦO, it can be observed that the % torque ripple is lowest for the proposed MTSDTC ONPWM for all speeds.

The torque ripple is comparatively reduced with TSDTC as compared to the proposed MTSDTC PWMON at a speed of 500rpm and 2000 rpm. From the plot, it can be concluded that the proposed MTSDTC ONPWM technique is one of the best DTC techniques among all which provides improved motor performance with reduced torque ripple under high and low-speed operation.

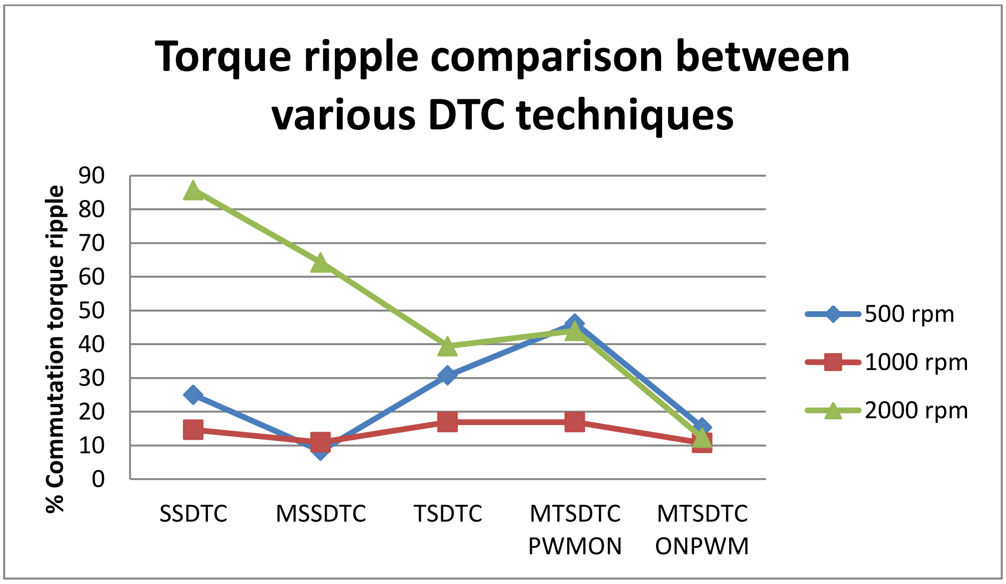

Fig. 4.37 Comparative plot showing % torque ripple for various DTC techniques

4.6 Conclusion

Direct torque control of BLDC motor requires no complex transformation of variables for closed-loop control of BLDC motor. Here, five different DTC techniques are simulated in MATLAB®/SIMULINK which includes two proposed PWMON and ONPWM control to provide a comparison of BLDC motor operation under 2-ΦO and 2-3ΦO. A comparative analysis of all the methods is shown to identify the most suitable DTC technique. The proposed modified twelve-step DTC control with PWMON and ONPWM control for closed-loop speed control of BLDC motor operates the motor below the rated speed in the constant torque region. The motor performance is tested under varied speed and load conditions. The comparison of the proposed ONPWM and PWMON control techniques is incorporated using the null vector concept with negative torque error in conduction as well as commutation region. The proposed technique reduces the switching losses along with the dead time elimination. The closed-loop speed control is accomplished by a finely tuned PI controller to improve the steady-state and dynamic performance of the drive. The simulation results indicate reduced conduction time and commutation torque ripple with the MTSDTC ONPWM technique as compared to the PWMON control for the same set speed and applied load conditions. The simulation results are validated by experimental results. The hardware results of the drive with the proposed technique under steady-state and dynamic operation prove its effectiveness under various speed and load conditions.